Fenton Reactions Drive Nucleotide and ATP Syntheses in Cancer

Huiyan Sun[1,2*], Chi Zhang[1,5*], Sha Cao[1,5], Tao Sheng[1], Ning Dong[1,4] and Ying Xu[1,2,3+]

[1]Computational Systems Biology Lab, Department of Biochemistry and Molecular Biology and Institute of Bioinformatics, University of Georgia, GA, USA, [2, 3]Colleges of Computer Science and Technology, and Public Health, [4]The First Hospital, Jilin University Medical School, Changchun, China. [5]Current Address: Center for Computational Biology and Bioinformatics, Department of Medical and Molecular Genetics and Biostatistics Department, Indiana University School of Medicine, IN, USA

A. SUPPLEMENTARY RESULTS

1. Observations from data analyses of cytosolic Fenton reactions

Extracellular superoxide is found to make substantial contributions to cytosolic Fenton reactions in BRCA, COAD, ESCA, HNSC, KIRC, KIRP, STAD, and THCA while mitochondrial superoxide has considerable contributions in BRCA, ESCA, KIRC, KIRP, LUAD, LUSC and STAD, based on our co-expression analyses. For the other four cancer types, contributions from either source is moderate.

Regarding the source of superoxide, we noted that the gene-expression levels of the NADH oxidases NOX1 and NOX4 in all cancer types correlate negatively with the predicted tumor purity of each sample with high statistical significance, as shown in Supplementary Figure S3, hence suggesting that these genes are expressed in immune or stromal cells rather than cancer cells. In addition, the expression levels of the VDAC genes significantly positively correlate with that of the mitochondrial superoxide dismutase SOD2 in the cancer types with significant contribution of mitochondrial superoxide in the fitted regression model, namely BRCA (p-value =1.62e^{-4}), KIRC (p-value = 3.71e^{-7}), KIRP (p-value = 4.28e^{-8}), LUAD (p-value = 1.64e^{-7}), and LUSC (p-value = 1.21e^{-6}), indicating that superoxide from mitochondria gets to cancer cell cytosols. Figure S4 shows the levels of correlation between the endogenous superoxide genes and the predicted level of cytosolic Fenton reaction as well as between the mitochondrial superoxide genes and the level of cytosolic Fenton reaction across the 14 cancer types. We can see from the figure that some cancers have higher correlations for the former while other cancers have higher correlations for the latter.

Gene-expression levels of cytosolic transferrin, ferritin and ferric reductases all show significant contributions to the strong correlation between the two sides of Eq. 13, indicating that a substantial amount of unreduced Fe^{3+} from cytosolic Fenton reactions is accumulated in cancer cytosol and hence contributing to overwhelming the pH buffer and changing its pH, where the predicted Fe^{3+} accumulation is consistent with published studies (Chen and Paw, 2012). In addition, gene-expression levels of transferrin and ferritin show positive and ferric reductases show negative correlations with the predicted levels of Fenton reactions, all supporting our prediction.

The two outcomes of Fe^{3+} as given in Eq. 10 and Eq. 11 that lead to OH^- accumulation correlate highly negatively with H^+ exporter genes, namely the SLC4A4-11 and SLC9, as shown in Figure S6. In addition, the predicted rates of OH^- production (Eq. 9) correlate at least as strongly with the expressions of both acid-loading and acid-extruding transporter genes: SLC4A-3, -4, -5, -s7, -9, -10, ATP2B-3, SLC9A-1, -6, -7, -9 and ATP6V-0A2, -0C, -0D2, -0E1, -0E2, -1A, -1E2, -1F, -1H, all with p-values < 0.05 by Mann Whitney test (detailed in Supplementary Figure S7), as the correlation between the predicted rates of hydroxyl radical production (predicted $[\cdot OH]'$ in Eq. 13) and the observed rate of $[\cdot OH]'$ in Eq. 13, measured using the expression levels of the marker genes for hydroxyl radical, all supporting our model.

2. Impact of cytosolic Fenton reactions on intracellular pH

Note from Figure S8 that the three main sources for cytosolic pyruvate production in cancer are glucose, malate originated from glutamine, and serine/glycine; and the five main effluxes from pyruvate are acetyl-CoA; oxaloacetate; amino acids alanine, lysine or aspartate; lactates; and sialic acids. Gene expression data analyses revealed that pyruvate production from glucose and serine is increased across all 14 cancer types, based on up-regulated glucose transporters, glycolytic enzymes, and serine dehydratase genes SDS and SDSL, which is consistent with the literature. In contrast, pyruvate effluxes as well as intracellular concentrations vary substantially across different cancers based on publicly available metabolomics data (Hirayama et al., 2009; Kami et al., 2013).

To assess *if all or only a fraction of the pyruvate produced through glycolysis goes towards lactic acid production and secretion*, we have conducted two random-effect linear regression analyses between the expression levels of the influx enzymes to pyruvate production *vs*. the efflux enzymes from pyruvate: one including the contribution of the gene-expressions of PKM2 & PKLR, and the other not. Lactate producing enzyme, LDHA, is considered as a random effect on the intercept, and the two linear models are compared based on the goodness of the fit.

Specifically, under the steady state assumption, we should have the total influx to pyruvate equal to the total efflux out of pyruvate; hence there should be non-negative values $\{ a_i \}$ that make the left and the right sides of the following approximately the same

$$a_1[\mathrm{PKM2}] + a_2[\mathrm{PKLR}] + a_3[\mathrm{ME1}] + a_4[\mathrm{SDS}] \approx a_5[\mathrm{NPL}] + a_6[\mathrm{GPT}] + a_7[\mathrm{PC}] + a_8[\mathrm{PDHA1}] + a_9[\mathrm{LDHA}]$$

where [X] represents the gene-expression level of protein X. For given tissue samples with available gene expression data, this problem can be formulated and solved as a non-negative least square problem. To control for contributions of glycolytic pyruvate to non-lactate efflux, we have discretized for each cancer type the $[\mathrm{LDHA}]$ expression values into three levels of equal subpopulations. In our regression model, the discretized LDHA expression is considered as a random effect affecting the linear model intercept.

To examine the contribution of $[\mathrm{PKM2}]$ and $[\mathrm{PKLR}]$ to the quality of this model, we built two random-effect linear regression models by holding the LDHA expression as a random effect that affects only the intercept: one with $[\mathrm{PKM2}]$ and $[\mathrm{PKLR}]$ as linear predictors, and the other without. For each cancer type, we compared the two models using Chi-Square test to see if adding the terms $[\mathrm{PKM2}]$ and $[\mathrm{PKLR}]$ could significantly improve the model fitting. We noted that for 7 out of 14 cancer types ($p < 0.05$) and for 10 out of 14 cancer types ($p < 0.07$) (Supplementary Table S1), adding the term significantly improves the linear model. Hence we conclude that glycolytic pyruvate makes substantial contributions to non-lactic metabolite syntheses in Figure S8.

To assess the amount of time needed for the protons associated with the glycolytic pyruvate to overwhelm the pH buffer, we have estimated the number of net protons needed to change the intracellular pH for one pH level, say, from 8.0 to 7.0. We assume that the

volume of a cancer cell is 100um^3, which is consistent with the published human cell data. For the intracellular pH to change from 8.0 to 7.0, the concentration of the H^+ needs to change from $10^{-8.0}$ to $10^{-7.0}$ mol/L. The following calculates the number of protons needed to make such a change for each such cell, assuming that the pH buffering coefficient of the cell is 2.0 x 10^5 for this pH range (Saleh et al., 1991):

$$(10^{-7.0} - 10^{-8.0}) \times 100 \times 2 \times 10^5 \times 10^{-15} \times 6.02 \times 10^{23} \cong 1.1 \times 10^9.$$

where 1L = 10^{15} um^3 and 6.02×10^{23} is the Avogadro constant. Hence, it takes 1.1×10^9 protons to make the desired pH change. It is known that proliferating human fibroblasts consume ~5 $\times 10^7$ glucose/second per cell (Flamholz et al., 2014). Using a conserved estimate, we assume that a cancer cell uptake 5×10^7 glucose/second, 50% of which goes to pyruvate but not involved in electron transport chain and at least 20% of these is not used towards lactate synthesis (and extracellular secretion). By putting these numbers together, we get: it takes ~220 seconds for such a cell to reach the desired pH change. While our estimate here might be crude, it highlights that it will not take long for Fenton reaction-infected cytosol to overwhelm the pH buffer and start to change the cytosolic pH.

3. Intracellular nucleotide concentration may drive cancer cell division?

It is not unthinkable that increased nucleotide concentration can drive DNA synthesis and cell division by cancer or cancer-forming cells, knowing that proliferation of prokaryotic cells and possibly all unicellular eukaryotic organisms such as yeast is driven by increased nucleotide or nucleotide-sugar concentration (Wang and Levin, 2009). For example, once ATP synthesis rate is higher than its consumption rate, the intracellular ATP concentration will continue to increase in such unicellular cells, resulting in slowdown of their ATP production and increase of nucleotide synthesis as the cells continue to consume the available nutrient. Cells like *E. coli* and yeast use intracellular nucleotide or nucleotide-sugar concentration as cue to activate DNA synthesis and cell-cycle progression. Hence we speculate that cancer cells may have utilized a similar program to activate the cell-division process to rid of their nucleotides (manuscript in preparation).

To probe further this issue, we have conducted a co-expression analysis between nucleotide synthesis and a few downstream pathways: DNA repair, DNA replication, RNA

POL I synthesis, aminoacyl-tRNA synthesis and cell cycle in the six cytosolic Fenton reaction harboring inflammatory diseases discussed and all 14 cancer types. The key information gained includes: (i) nucleotide synthesis is not strongly correlated with cell-cycle progression in the six inflammatory diseases; (ii) while they are more correlated in cancers, the correlation level spans a wide range across different cancers and is not nearly as strong as that with DNA repair, strongly suggesting that nucleotide synthesis, DNA synthesis and cell-cycle progression are not coordinated through regulation as in normal proliferating cells in human tissues; and (iii) nucleotide synthesis strongly correlates with DNA repair in both inflammatory diseases and cancers, suggesting that DNA repair may be a key inducer of nucleotide synthesis. Hence, we posit that it is DNA repair processes that may induce nucleotide synthesis rather than DNA replication, which is clearly different from the typical proliferation process where the need for DNA replication drives nucleotide synthesis. The details are given in Supplementary Table S3.

4. Observations from data analyses of mitochondrial Fenton reactions

The mitochondrial NADH and superoxide contribute strongly to the reduction of Fe^{3+} from mitochondrial Fenton reactions, hence driving the continuous Fenton reactions. In parallel, significant Fe^{3+} accumulation and its correlation with mitochondrial Fenton reactions are also observed based on the up-regulated mitochondrial iron importer genes SLC25A28 and SLC25A37, heme synthesis gene ALAS1 and their significant correlations with protein damages in mitochondria, indicating that some OH^- produced by mitochondrial Fenton reactions are not naturalized by Fenton or associated reactions, hence leading to consumption of protons inside mitochondria.

The expression levels of Complexes I and III both show strong correlations with our predicted levels of the mitochondrial Fenton reactions when Fe^{3+} being reduced by superoxide or unreduced. Interestingly, higher correlations were observed in cancer tissues with higher levels of hypoxia, measured using the expression levels of hypoxia marker genes EGLN1 and EGLN3, as detailed in Supplementary Methods and Figure S12.

The expression levels of ATP-ADP exchanger genes SLC25A4, SLC25A5 and SLC25A6 all show strong correlations with the predicted rates of mitochondrial Fenton

reactions when Fe^{3+} being reduced by superoxide or unreduced, strongly suggesting that such Fenton reactions contribute to ATP syntheses. Similarly, higher correlations are observed in cancer tissues that are more hypoxic, which are particularly so for cancer types with significant levels of mitochondrial Fenton reactions, namely BRCA, COAD, KICH, KIRC, KIRP, LUAD and PRAD, suggesting that some aerobic respiration may take place in O_2 rich environment as in normal cells.

One evidence for unreduced Fe^{3+} in mitochondria is the increased synthesis of iron-sulfur clusters as reflected by the HSCB gene and the ABCB6 gene, the former of which transfers a newly synthesized iron-sulfur to specific proteins and the latter removes iron sulfur from the mitochondria, as shown in Figure S14. The rationale is that a damaged iron-sulfur cluster indicates that Fenton reaction already takes place, hence Fe^{2+} is oxidized to Fe^{3+} and then the iron-sulfur cluster is replaced by a new one while the Fe^{3+} ions along with the damaged iron-sulfur cluster will be removed from mitochondria using the ABCB6 transporter (Richardson et al., 2010). From the figure, we can see both genes are up-regulated in majority of the cancer types, indicating the number of unreduced Fe^{3+} is increased.

5. Additional evidence for UCP5 being used for ATP production

Strong positive correlations between UCP5 and mitochondrial iron importer genes SLC25A28 and SLC25A37 while negative correlation between UCP5 and the rate-limiting gene ALAS1 of heme synthesis are observed in BRCA, HNSC, KIRC, KIRP, LUAD, PRAD and THCA but not in normal tissues. These observations suggest that the activation of UCP5 is associated with the accumulation of Fenton reaction-produced Fe^{3+}, but not Fe^{2+}.

Furthermore, the malate importer gene SLC25A11 of the malate-aspartate shuttle is largely up-regulated and strongly co-expressed with Fe^{3+} accumulation rather than the aspartate anti-porter SLC25A12 in cancer. Noting that previous studies have discovered that malate accumulation in cancer cells of multiple cancer types where malate serves as a chelator of Fe^{3+} (Hamada et al., 2005). Hence, we posit that the unreduced Fe^{3+} produced by mitochondrial Fenton reactions are chelated with malate and accumulated in mitochondria, which directly contribute to cross-membrane proton gradients and ATP synthesis.

B. SUPPLEMENTARY METHODS

1. Comparative analyses of Fenton reactions in cancer *vs.* inflammatory disease

Comparitive analyses of the differentially expressed genes in 16 types of inflammatory diseases and the 14 cancer types are made. Differentially expressed genes are identifed in each dataset by using Mann-Whitney test with FDR < 0.05 as the significance cutoff. Considering that the cancer transcriptomic data are all measured using RNA-seq while only microarray data are avialable for the inflammatory diseases, we have also included 12 of the 14 cancer types measured by the same micorarray platform to assure that most of the differentially expressed genes discussed in this study are consistantly identified in both data types.

2. Differential gene expression and pathway enrichment

Differential gene expression is assessed by using the Mann-Whitney test on the RSEM (or RPKM) normalized RNA-seq data collected from cancer *vs*. control samples of each cancer type. FDR is applied to control false discoveries and FDR < 0.005 is used as the significance cutoff for determining differential gene expression.

Pathway enrichment analysis is conducted and the statistical significance of each enriched pathway is assessed by using a hypergeometric test (statistical significance cutoff = 0.005) against pathways retrieved from GO and MsigDB as well as ~40 manually curated Fenton reaction related gene sets (Subramanian et al., 2005).

3. Genes selected for estimation of Fenton reactions in mitochdondria and ECM

Mitochondrial Fenton reaction: The gene-expression levels of up-regulated protein-degradation enzymes in mitochondria, specifically CLPP, LONP1, THOP1, HTRA2, PMPCA, PMPCB, SPG7, CLPX, and AFG3L2 are used to estimate the mitochondrial $[\cdot OH]$. All mitochondrial iron-sulfur proteins are used as the source of F_e^2 accessible to mitochondrial Fenton reactions; and hence $[Fe^{2+}]$ is estimated by using a linear model of expressions of the synthesis genes of iron-sulfur clusters, namely CIAO1, BRIP1, HSPA9 and ACO2. Mitochondrial $[H_2O_2]$ is estimated using a linear model over the expressions of mitochondrial anti-oxidation reductases such as GPX4 and TXN. The level of reducing agents, [RA], is

estimated by using the expression data of mitochondrial dehydrogenases. The level of superoxide, $[O_2^{\cdot -}]$, is estimated using the gene-expressions of mitochondrial superoxide dismutase SOD2. Fe^{3+} accumulation is estimated using mitochondrial iron transporter genes SLC25A28 and SLC25A37, the rate-limiting enzyme of iron-sulfur cluster synthesis ISCU and the rate-limiting enzyme of heme synthesis ALAS1.

Extracellular matrix Fenton reaction: $[\cdot OH]$ is estimated using ECM degradation genes MMPs (Supplementary Table S1) via a regression model over $[H_2O_2]$ and $[C_u^{1+}]$ since C_u instead of F_e is involved in such Fenton reactions. $[H_2O_2]$ is estimated using the expressions of NOX2, NOX3 and GPX7 while $[C_u^{1+}]$ is estimated by using the expressions of two extracellular copper-dependent enzymes: lysyl oxidase (LOX) and lysyl oxidase like 2 (LOXL2). It has been reported that the copper(I) ions in lysyl oxidase are involved in Fenton reaction and the produced copper(II) ions can be further reduced by superoxide: $Cu^+ + H_2O_2$ -> $Cu^{2+} + \cdot OH + OH^-$; $Cu^{2+} + O_2^{\cdot -}$ -> $Cu^+ + O2$; and $Cu^+ + O_2^{\cdot -} + 2H^+$ -> $Cu^{2+} + H_2O_2$ (Brown Jr, 1997). It is noteworthy that all the genes used to assess extracellular Fenton reactions are genes expressed in stromal and local immune cells rather than cancer cells.

4. Inference of subcellular location of selected proteins

The subcellular location of a protein is first predicted based on the annotation in Genecards, which uses a number between 0 and 5 to represent the reliability of a prediction, with 5 being the most confident and 0 being the least. We have used 4 as the cutoff in assessing the subcellular localization for a protein (Safran et al., 2010).

5. Hypoxia level prediction

We have previously developed a computational method to estimate the oxidative stress level of a tissue sample based on expression levels of ~40 genes whose proteins either contribute to the generation of oxidative stress or respond to it (Cao et al., 2015). Here, a similar approach is applied to train a predictor for the hypoxic level in the given tissue based on its gene expression data. Specifically, we have collected 10 gene-expression datasets of 24 samples with known hypoxia levels and 30 control samples as the training data (see Supplementary Table S4) to train a predictor for the microarray data (Affymetrix UA133 plus

2.0 array). 180 genes are selected as hypoxia responsive genes, including known hypoxia induce factor I and II (HIF1 and HIF2) and genes directly regulated by them, retrieved from the *Transfec* database (Wingender et al., 1996) and genes annotated by GO to be hypoxia responsive. The predictor is trained by using a logistic regression model with variable selection by using L1 regularization(Park and Hastie, 2007). "glmnet" in the R package is applied to train the predictor and the model parameters are selected that achieve the highest prediction accuracy with 10-fold cross-validation. Five genes, namely EGLN1, EGLN3, MAT2A, PFKFB3 and PFKFB4, are selected and used in the final predictor, which achieves 96.1% prediction accuracy in 10-fold cross validation.

To predict the hypoxia level of a tissue sample based on the RNA-seq data, we have selected gene EGLN3 (Egl-9 Family Hypoxia Inducible Factor 3) with the highest F score among the five selected genes in the logistic regression-based prediction model. A higher expression level of EGLN3 implies a more hypoxic condition. We have used the expression level of EGLN3 to classify the samples of each cancer type into *hypoxic* (top 30% EGLN3 expressed samples), *aerobic* (bottom 30% EGLN3 expressed samples) and *intermediate* groups.

The non-linear model for Fenton reaction in each subcellular location is fitted with gene-expression data in each hypoxia group, respectively. The predicted mitochondrial Fenton reaction levels in each group strongly correlate with the ETC Complex I and III genes for each cancer type. Consistently higher correlations ($p < 1e\text{-}5$ by Mann-Whitney test) between the predicted Fenton reaction level and ETC Complex I and III genes in samples with higher hypoxia levels are observed in all cancer types with significant mitochondrial Fenton reactions, namely BLCA, BRCA, COAD, KICH, KIRC, KIRP, LUAD, LUSC, PRAD, and STAD. Detailed correlations between predicted Fenton reaction level and ETC Complex I and III genes in different hypoxia groups and cancer types are shown in Supplementary Figure S12.

6. Prediction of tumor purity

To assure that the analyzed extracellular genes are truly expressed by stromal or immune cells rather than cancer cells, we have selected genes with expression levels

negatively correlated with the cancer purity predicted by ESTIMATE, ABSOLUTE, LUMP, IHC and CPE methods in each of the 14 cancer types (Aran et al., 2015). Detailed correlations between the gene expression and predicted cancer purity are given in Supplementary Figure S3.

7. Validation of saturated malate-aspartate (M-A) shuttle

The net result of M-A shuttle is to regenerate NAD+ in cytosol and produce NADH in mitochondria. In this process, SLC25A11 transports malate into mitochondria and SLC25A12/SLC25A13 transport aspartate out of mitochondria. In normal conditions with balanced NADH and NAD+, there should be a strong correlation between the expressions of SLC25A11 and SLC25A12/SLC25A13. Interestingly, the correlation is insignificant in cancer tissues in general across 14 cancer types. Furthermore, we noted that SLC25A11 strongly correlates with ETC Complex I, which is the first step to utilize NADH to transport electron, but the correlation between SLC25A12/SLC25A13 and Complex I is insignificant. This strongly suggests that the transportation rates of SLC25A12/SLC25A13 reach their maximum, i.e., they become saturated while SLC25A11 remains at a high rate. Previous studies have shown that the efflux of aspartate is irreversible and the rate-limiting step of the M-A shuttle, while the exchange between malate and α-ketoglutarate is driven by the concentration gradients of its substrates. By integrating all these, we predict that malate is being used to chelate Fe^{3+} (Lu et al., 2008; Adam et al., 2015).

8. Variable selection and statistical significance test

"glmnet" in R package is applied to compute each regression model with variable selection by using a L1-penalty (Friedman et al., 2010). Cross-validation is applied to achieve the best λ value for each fitting. To assess the statistical significance of each regression model, we conducted a permutation-based testing by using the following criteria: (i) R^2 value, (ii) the number of selected variables, (iii) biological explanation of the positive or negative sign of each model parameter, and (iv) biological meaning of each gene used. A p-value < 0.005 is used as the cutoff for the statistical significance.

9. Assessment of statistical significance of Fenton reaction prediction

For each regression model of each Fenton reaction related quantity, statistical significance from three aspects is assessed to demonstrate the occurrence of a Fenton reaction: (i) over expression of each Fenton reaction associated gene; (ii) significance in fitting the reaction equation, Eq. 13 in the main text, calculated using a permutation test on the R^2 value by randomly choosing the same number of genes with similar expression patterns to those used for estimating [Fe^{2+}], [H_2O_2], [$\bullet OH$], [O_2^-] and [RA], respectively, for variable selection; and (iii) the sign of each regression parameter, which is assessed using a permutation test on a predefined Sign-Score, and 0.005 was used as the cutoff for the significance values. For (i) and (ii), we have applied a test by permuting the independent variables in the regression model and another test to permute the dependent variables by fitting the regression model against genes with similar over-expression levels but independent of those of the selected marker genes for $[\cdot OH]$ production.

Our analysis indicates that Eq. 13 is non-linear. Hence a polynomial model based on Tayler expansion of the function is used to capture the non-linear relationship. The non-linear function is first approximated using a linear regression over a set of expanded variables based on the Taylor expansion. Genes deemed to make significant contributions are selected using a linear regression with an L1-penalty. Then a non-linear regression of the selected genes is then conducted.

The sign of the regression parameters is defined by the following function to assess the significance for the occurrence of Fenton reaction in a specific subcellular location:

$$\text{Sign Score} = \frac{\sum_{\text{RA}} (\text{K}_1^{\text{RA}} + \text{K}_2^{\text{RA}} + \text{K}_3^{\text{RA}} + \text{K}_{\text{cat}}^{\text{RA}} + \text{K}_5^{O_2^-} + \text{K}_6^{O_2^-} + \text{K}_7^{O_2^-} + \text{K}_{\text{cat}}^{O_2^-})}{\sum_{\text{RA}} (|\text{K}_1^{\text{RA}}| + |\text{K}_2^{\text{RA}}| + |\text{K}_3^{\text{RA}}| + |\text{K}_{\text{cat}}^{\text{RA}}| + |\text{K}_5^{O_2^-}| + |\text{K}_6^{O_2^-}| + |\text{K}_7^{O_2^-}| + |\text{K}_{\text{cat}}^{O_2^-}|)}$$

The significance of the Sign Score is assessed using a permutation test. P-value = 0.005 is used as the significance cutoff.

10. Pathway-pathway correlation significance calculation

For two pathways P1 and P2 with p1 and p2 genes, respectively, we have calculated their Pearson correlation and constructed a correlation p1 x p2 matrix. We then counted all the gene pairs which satisfy: (a) p-value < 0.01 and (b) correlation value is above 0.1. We

have then conducted 10,000 permutations of the two pathways. Let N be the number of such pairs and M the number of times out of these permutation tests with significant gene pairs at least being N. The following is used as the significance value:

$$\text{Permutation pvalue} = \frac{\text{M}}{10000}$$

11. Validation of up-regulated gene expressions against protein expression data

All the up-regulated genes in cancer tissues used in this study are validated using protein expression data in the relevant cancer type. The staining data for 16,236 proteins in 14 types of human cancers are retrieved from The Human Protein Atlas. For most proteins, they have four staining level: high, middle, low and not detectable, which are scored as 5, 3, 1 and 0, respectively. Since the database also contains the following information: the number of patients for each of these four levels for each protein and the total number of patients included for each cancer type, we can calculate the proportion of this protein in different levels and derive its staining score as defined above.

8 of the 14 cancer types used in our study are included in this database: BRCA, HNSC, LUSC, STAD, COAD, LIHC, PRAD and THCA. For each cancer type, we compared average staining scores for each protein in each cancer type, and consider up-, down-regulation or change for protein in each cancer type, when assessing the consistencies between differential gene expressions and protein abundance data.

C. SUPPLEMENTARY FIGURES AND CAPTIONS

Figure S1: Elevated iron level in cancer *vs.* control across 14 cancer types (the x-axis). The y-axis is the axis of genes involved in iron uptake, usage and storage. Each entry is the log2-transformed fold-change averaged over all samples of cancer *vs.* control, where blue is for up and red for down-regulation with the detailed color scheme given in the top panel. Eight genes are used with TFR2 for transferrin receptor 2; TFRC for transferrin receptor; STEAP3 for STEAP family member 3; SLC25A37 for solute carrier family 25, member 37; FTH1 for ferritin, heavy polypeptide 1; HAMP for hepcidin antimicrobial peptide, and SLC40A1 for solute carrier family 40 (iron-regulated transporter), member 1, an iron exporter.

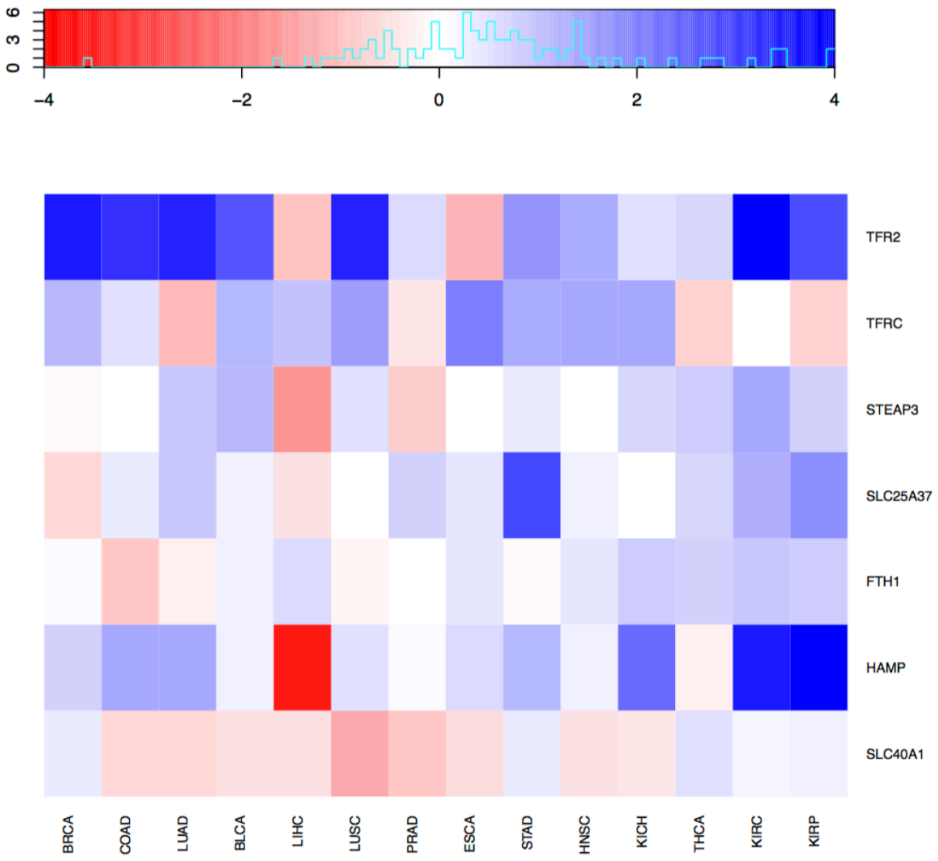

Figure S2: Elevated H_2O_2 level in cancer *vs.* control across 14 cancer types (the x-axis). The y-axis is the axis of genes reflecting the H_2O_2 level. Each entry is the log2-transformed fold-change averaged over all samples of cancer *vs.* control, where the color scheme is the same as in Figure S1. Thirteen genes are used with GCLC for glutamate-cysteine ligase, catalytic subunit; GPX1 for glutathione peroxidase 1; GCLM for glutamate-cysteine ligase, modifier subunit; GPX5 for glutamate-cysteine ligase, modifier subunit 5; GPX7 for glutamate-cysteine ligase, modifier subunit 7; TXN for thioredoxin; GPX8 for glutamate-cysteine ligase, modifier subunit 8; GPX4 for for glutamate-cysteine ligase, modifier subunit 4; GPX2 for glutamate-cysteine ligase, modifier subunit 2; and TXNRD1 for thioredoxin reductase 1.

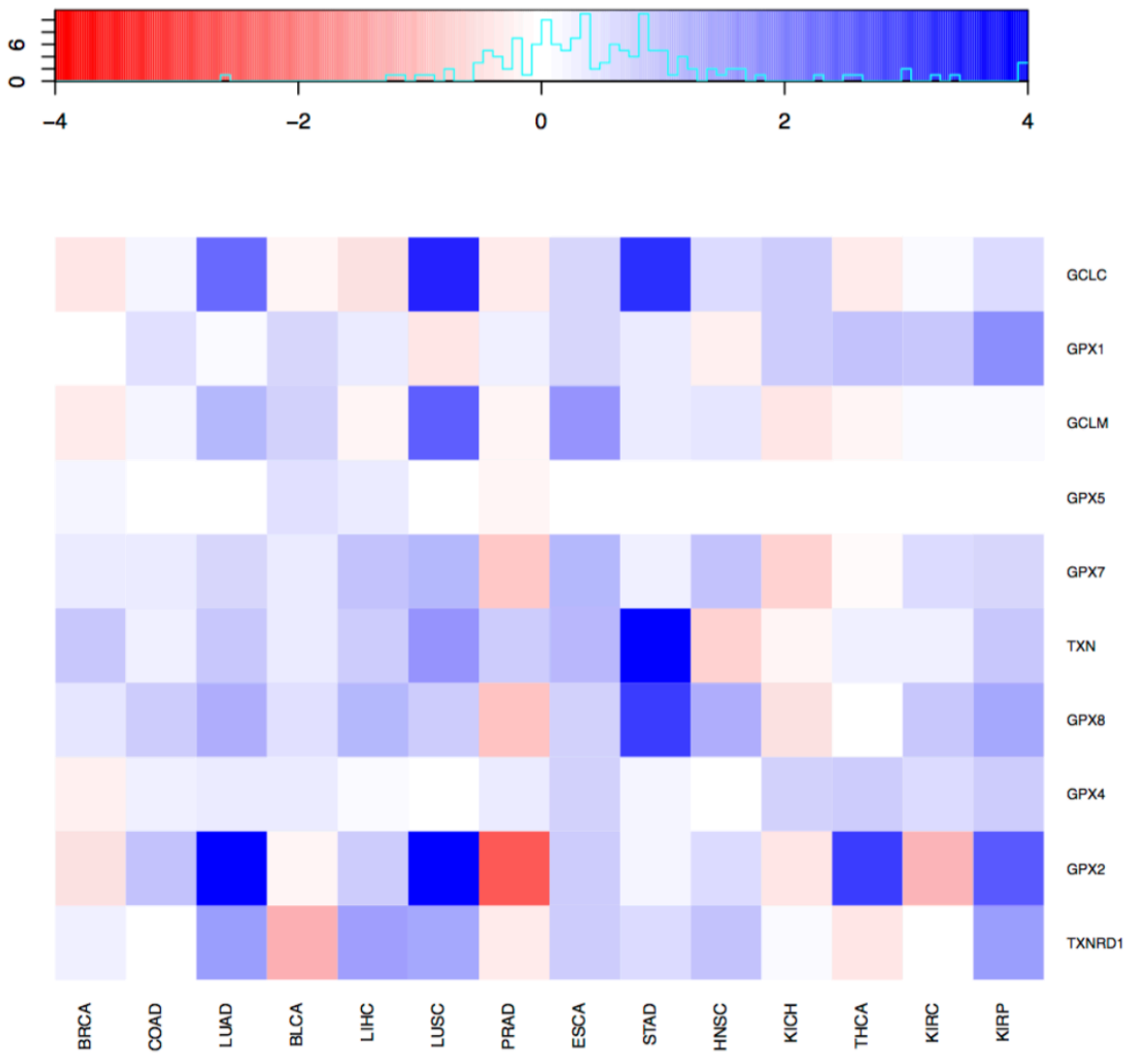

Figure S3: Correlation between the expression levels of extracellular genes and the predicted cancer tissue purities. Cancer sample purities predicted by five methods in the public domain are used. Consistent negative correlations between the predicted purity and the expressions of certain extracellular genes are observed. "-" means not available.

NOX4


−0.59 −0.35 −0.21 −0.31 −0.42 BLCA
−0.43 −0.27 − −0.19 −0.28 BRCA
−0.74 −0.47 −0.31 −0.12 −0.58 COAD
−0.52 −0.34 −0.01 −0.19 −0.35 HNSC
−0.01 − 0.12 0.11 0.04 KICH
−0.05 −0.13 −0.04 −0.08 −0.1 KIRC
−0.21 − −0.14 −0.18 −0.15 KIRP
−0.38 − −0.14 −0.15 −0.23 LIHC
−0.38 −0.35 −0.22 −0.14 −0.35 LUAD
−0.46 −0.33 −0.17 −0.28 −0.32 LUSC
−0.53 − −0.28 −0.05 −0.33 PRAD
−0.35 − −0.2 −0.14 −0.25 THCA
ESTIMATE
ABSOLUTE
LUMP
IHC
CPE

NOX1

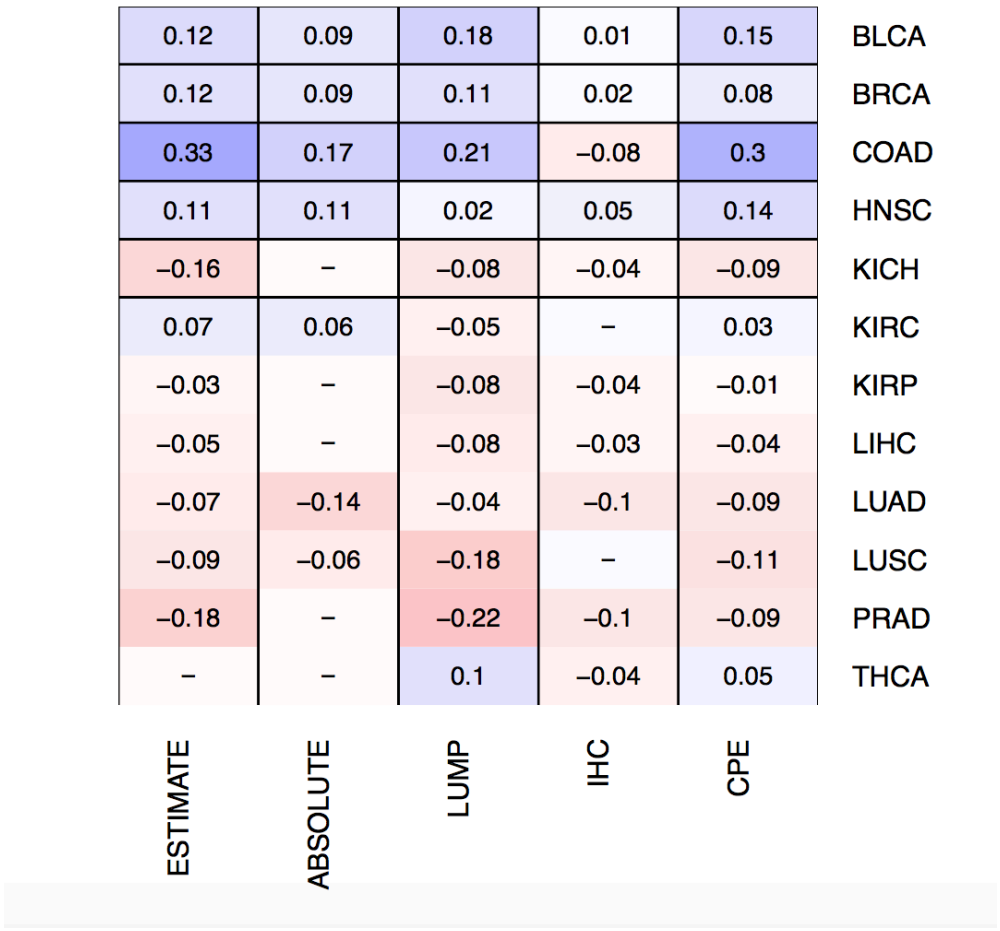
0.12 0.09 0.18 0.01 0.15 BLCA
0.12 0.09 0.11 0.02 0.08 BRCA
0.33 0.17 0.21 −0.08 0.3 COAD
0.11 0.11 0.02 0.05 0.14 HNSC
−0.16 − −0.08 −0.04 −0.09 KICH
0.07 0.06 −0.05 − 0.03 KIRC
−0.03 − −0.08 −0.04 −0.01 KIRP
−0.05 − −0.08 −0.03 −0.04 LIHC
−0.07 −0.14 −0.04 −0.1 −0.09 LUAD
−0.09 −0.06 −0.18 − −0.11 LUSC
−0.18 − −0.22 −0.1 −0.09 PRAD
− − 0.1 −0.04 0.05 THCA
ESTIMATE
ABSOLUTE
LUMP
IHC
CPE

NOX5

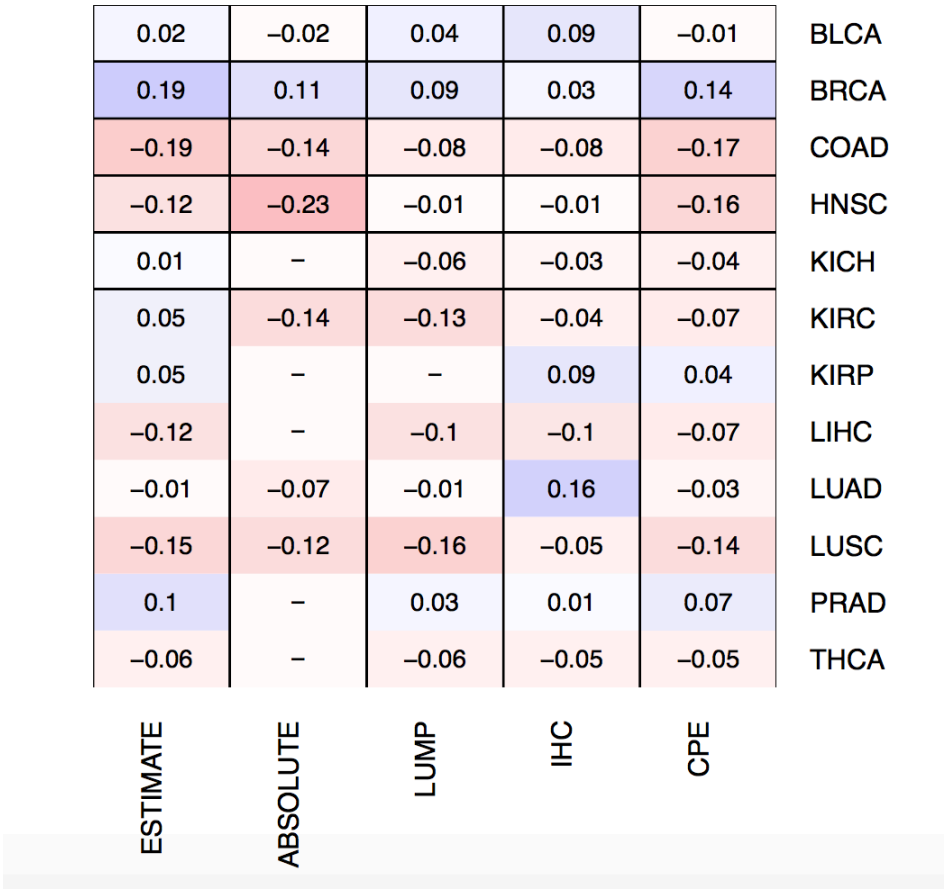
0.02 −0.02 0.04 0.09 −0.01 BLCA
0.19 0.11 0.09 0.03 0.14 BRCA
−0.19 −0.14 −0.08 −0.08 −0.17 COAD
−0.12 −0.23 −0.01 −0.01 −0.16 HNSC
0.01 − −0.06 −0.03 −0.04 KICH
0.05 −0.14 −0.13 −0.04 −0.07 KIRC
0.05 − − 0.09 0.04 KIRP
−0.12 − −0.1 −0.1 −0.07 LIHC
−0.01 −0.07 −0.01 0.16 −0.03 LUAD
−0.15 −0.12 −0.16 −0.05 −0.14 LUSC
0.1 − 0.03 0.01 0.07 PRAD
−0.06 − −0.06 −0.05 −0.05 THCA
ESTIMATE
ABSOLUTE
LUMP
IHC
CPE

LOX


−0.62 −0.48 −0.33 −0.35 −0.46 BLCA
−0.48 −0.33 −0.14 −0.2 −0.35 BRCA
−0.73 −0.42 −0.29 −0.12 −0.55 COAD
−0.3 −0.14 0.02 −0.07 −0.18 HNSC
−0.38 − −0.35 −0.11 −0.36 KICH
−0.38 −0.34 −0.22 −0.06 −0.34 KIRC
−0.35 − −0.37 −0.16 −0.33 KIRP
−0.26 − −0.25 −0.19 −0.26 LIHC
−0.47 −0.38 −0.25 −0.11 −0.41 LUAD
−0.42 −0.36 −0.23 −0.2 −0.34 LUSC
−0.07 − −0.04 −0.06 −0.06 PRAD
−0.4 − −0.35 −0.24 −0.36 THCA
ESTIMATE
ABSOLUTE
LUMP
IHC
CPE

LOXL2

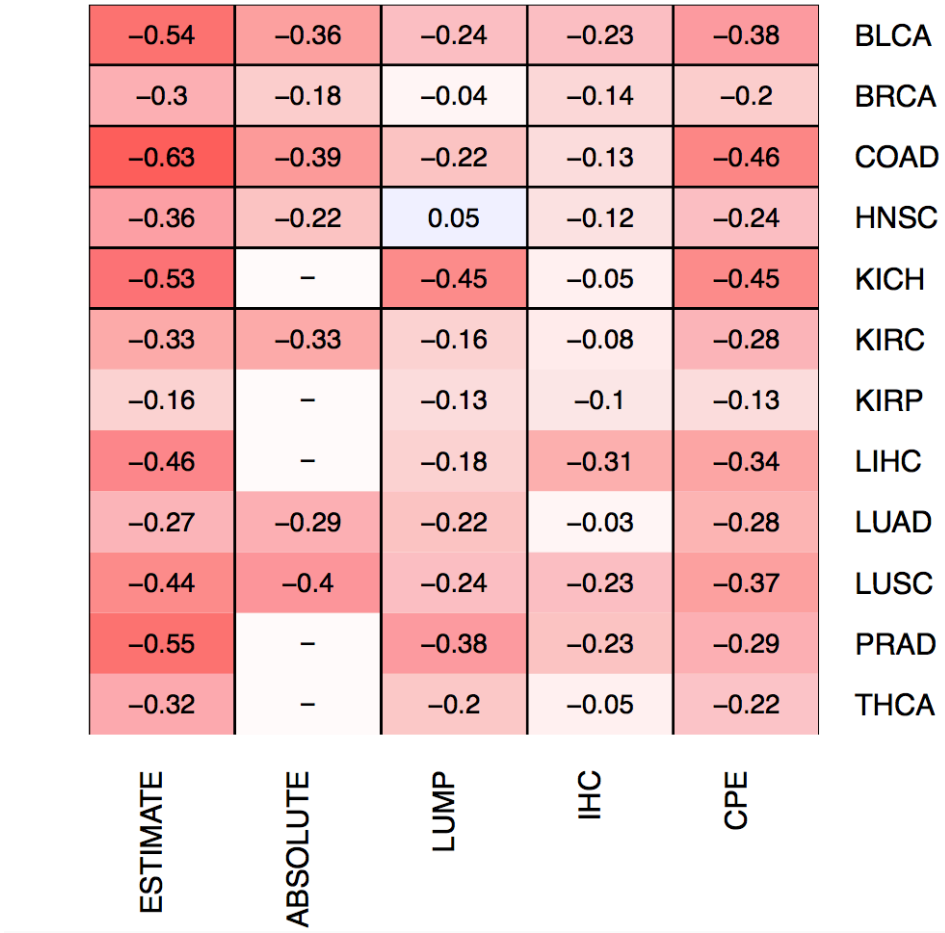
−0.54 −0.36 −0.24 −0.23 −0.38 BLCA
−0.3 −0.18 −0.04 −0.14 −0.2 BRCA
−0.63 −0.39 −0.22 −0.13 −0.46 COAD
−0.36 −0.22 0.05 −0.12 −0.24 HNSC
−0.53 − −0.45 −0.05 −0.45 KICH
−0.33 −0.33 −0.16 −0.08 −0.28 KIRC
−0.16 − −0.13 −0.1 −0.13 KIRP
−0.46 − −0.18 −0.31 −0.34 LIHC
−0.27 −0.29 −0.22 −0.03 −0.28 LUAD
−0.44 −0.4 −0.24 −0.23 −0.37 LUSC
−0.55 − −0.38 −0.23 −0.29 PRAD
−0.32 − −0.2 −0.05 −0.22 THCA
ESTIMATE
ABSOLUTE
LUMP
IHC
CPE

GPX7

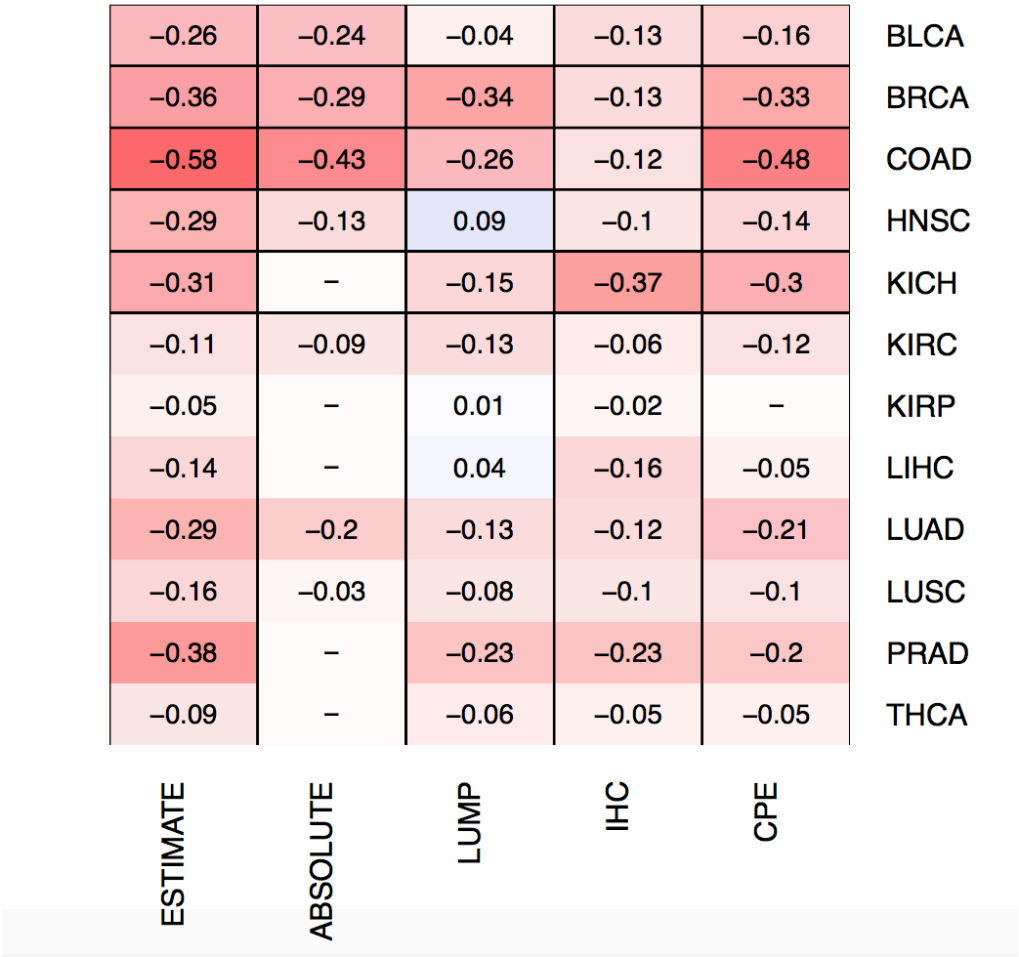
−0.26 −0.24 −0.04 −0.13 −0.16 BLCA
−0.36 −0.29 −0.34 −0.13 −0.33 BRCA
−0.58 −0.43 −0.26 −0.12 −0.48 COAD
−0.29 −0.13 0.09 −0.1 −0.14 HNSC
−0.31 − −0.15 −0.37 −0.3 KICH
−0.11 −0.09 −0.13 −0.06 −0.12 KIRC
−0.05 − 0.01 −0.02 − KIRP
−0.14 − 0.04 −0.16 −0.05 LIHC
−0.29 −0.2 −0.13 −0.12 −0.21 LUAD
−0.16 −0.03 −0.08 −0.1 −0.1 LUSC
−0.38 − −0.23 −0.23 −0.2 PRAD
−0.09 − −0.06 −0.05 −0.05 THCA
ESTIMATE
ABSOLUTE
LUMP
IHC
CPE

NCF1

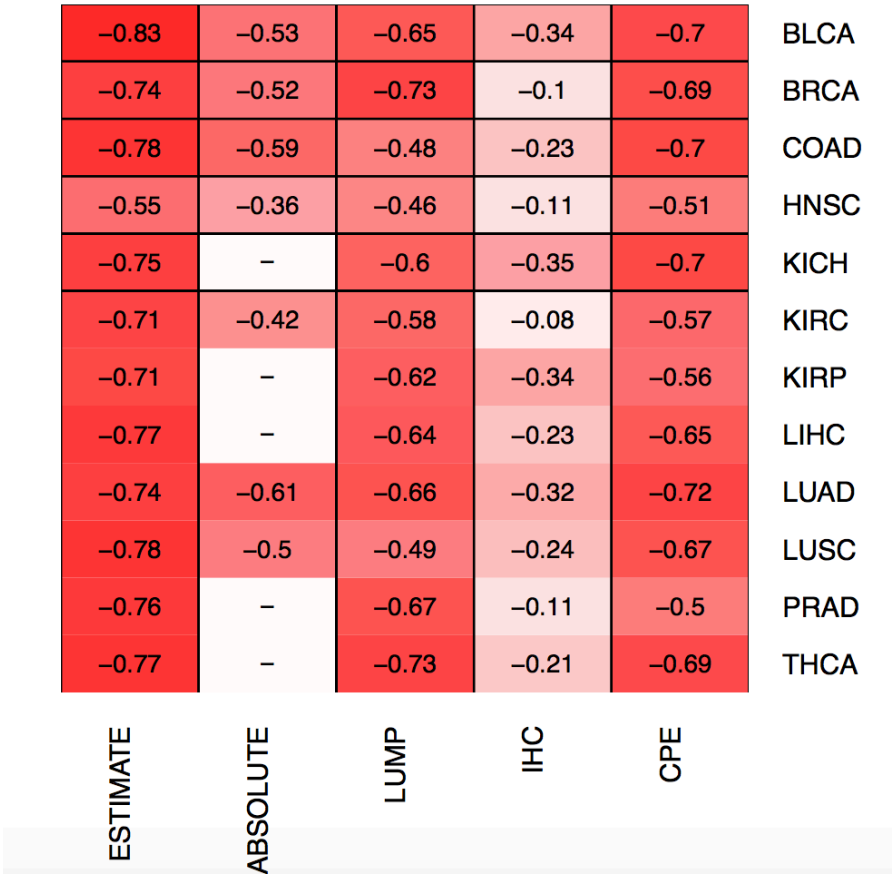
−0.83 −0.53 −0.65 −0.34 −0.7 BLCA
−0.74 −0.52 −0.73 −0.1 −0.69 BRCA
−0.78 −0.59 −0.48 −0.23 −0.7 COAD
−0.55 −0.36 −0.46 −0.11 −0.51 HNSC
−0.75 − −0.6 −0.35 −0.7 KICH
−0.71 −0.42 −0.58 −0.08 −0.57 KIRC
−0.71 − −0.62 −0.34 −0.56 KIRP
−0.77 − −0.64 −0.23 −0.65 LIHC
−0.74 −0.61 −0.66 −0.32 −0.72 LUAD
−0.78 −0.5 −0.49 −0.24 −0.67 LUSC
−0.76 − −0.67 −0.11 −0.5 PRAD
−0.77 − −0.73 −0.21 −0.69 THCA
ESTIMATE
ABSOLUTE
LUMP
IHC
CPE

NCF2

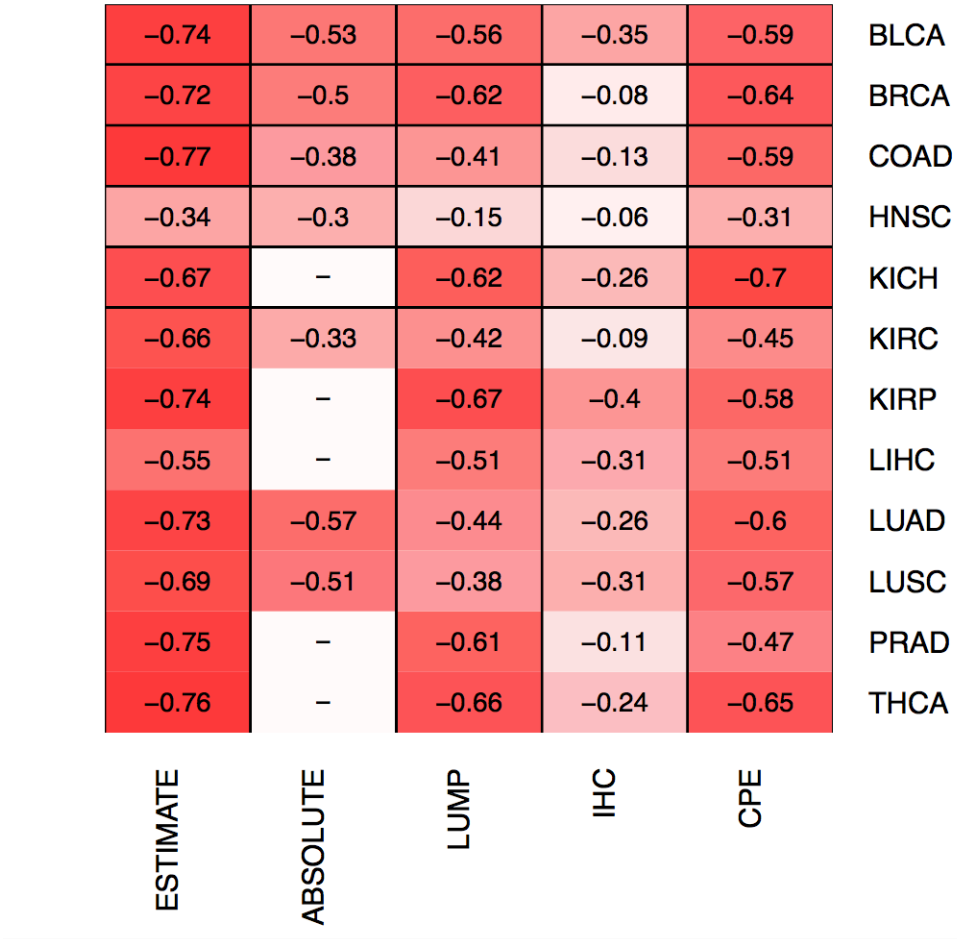
−0.74 −0.53 −0.56 −0.35 −0.59 BLCA
−0.72 −0.5 −0.62 −0.08 −0.64 BRCA
−0.77 −0.38 −0.41 −0.13 −0.59 COAD
−0.34 −0.3 −0.15 −0.06 −0.31 HNSC
−0.67 − −0.62 −0.26 −0.7 KICH
−0.66 −0.33 −0.42 −0.09 −0.45 KIRC
−0.74 − −0.67 −0.4 −0.58 KIRP
−0.55 − −0.51 −0.31 −0.51 LIHC
−0.73 −0.57 −0.44 −0.26 −0.6 LUAD
−0.69 −0.51 −0.38 −0.31 −0.57 LUSC
−0.75 − −0.61 −0.11 −0.47 PRAD
−0.76 − −0.66 −0.24 −0.65 THCA
ESTIMATE
ABSOLUTE
LUMP
IHC
CPE

NCF4

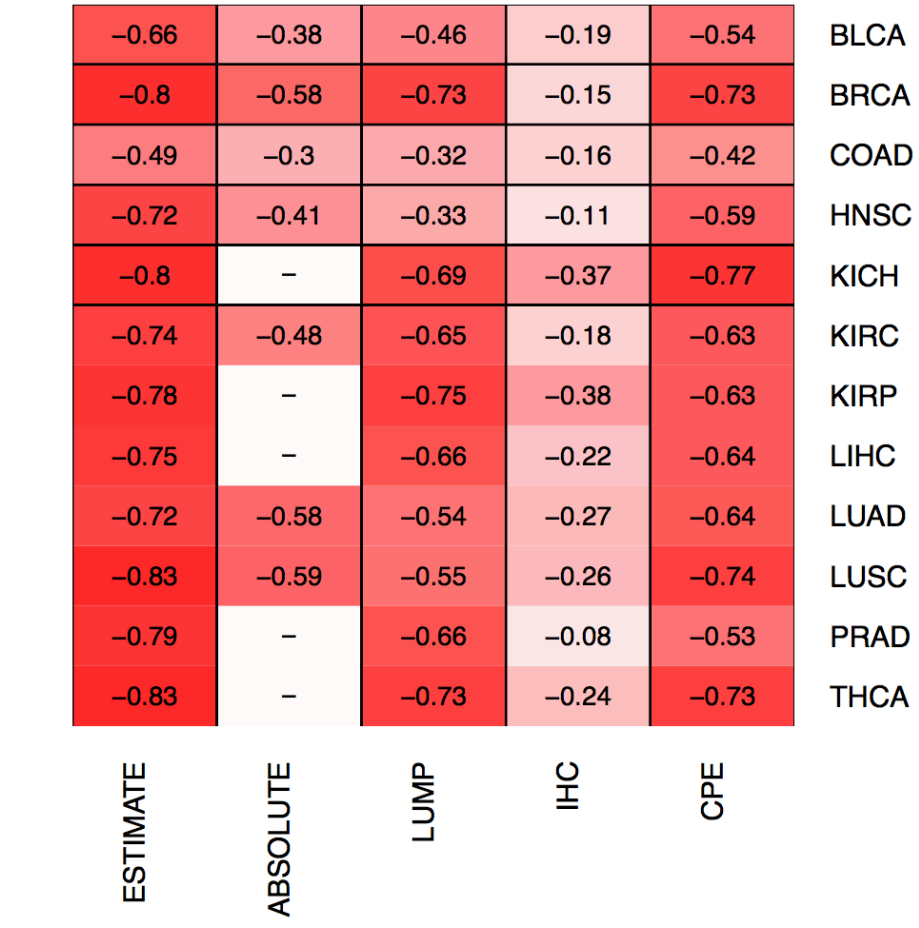
−0.66 −0.38 −0.46 −0.19 −0.54 BLCA
−0.8 −0.58 −0.73 −0.15 −0.73 BRCA
−0.49 −0.3 −0.32 −0.16 −0.42 COAD
−0.72 −0.41 −0.33 −0.11 −0.59 HNSC
−0.8 − −0.69 −0.37 −0.77 KICH
−0.74 −0.48 −0.65 −0.18 −0.63 KIRC
−0.78 − −0.75 −0.38 −0.63 KIRP
−0.75 − −0.66 −0.22 −0.64 LIHC
−0.72 −0.58 −0.54 −0.27 −0.64 LUAD
−0.83 −0.59 −0.55 −0.26 −0.74 LUSC
−0.79 − −0.66 −0.08 −0.53 PRAD
−0.83 − −0.73 −0.24 −0.73 THCA
ESTIMATE
ABSOLUTE
LUMP
IHC
CPE

NCF1C

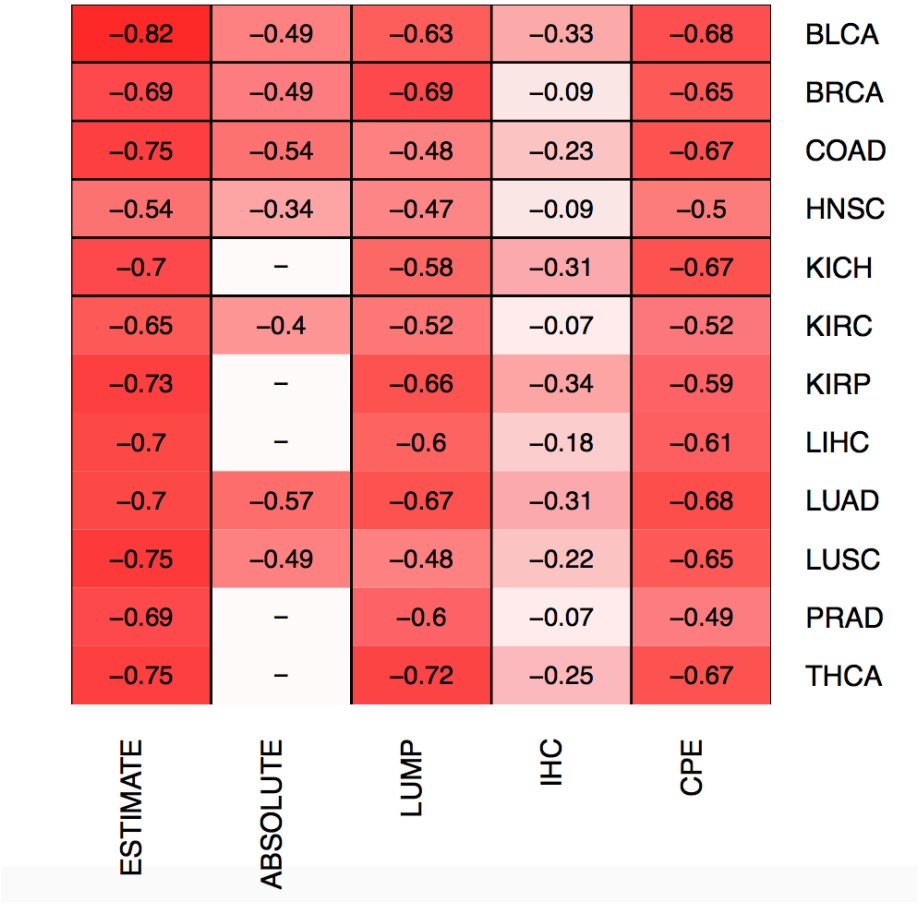
−0.82 −0.49 −0.63 −0.33 −0.68 BLCA
−0.69 −0.49 −0.69 −0.09 −0.65 BRCA
−0.75 −0.54 −0.48 −0.23 −0.67 COAD
−0.54 −0.34 −0.47 −0.09 −0.5 HNSC
−0.7 − −0.58 −0.31 −0.67 KICH
−0.65 −0.4 −0.52 −0.07 −0.52 KIRC
−0.73 − −0.66 −0.34 −0.59 KIRP
−0.7 − −0.6 −0.18 −0.61 LIHC
−0.7 −0.57 −0.67 −0.31 −0.68 LUAD
−0.75 −0.49 −0.48 −0.22 −0.65 LUSC
−0.69 − −0.6 −0.07 −0.49 PRAD
−0.75 − −0.72 −0.25 −0.67 THCA
ESTIMATE
ABSOLUTE
LUMP
IHC
CPE

NCF1B

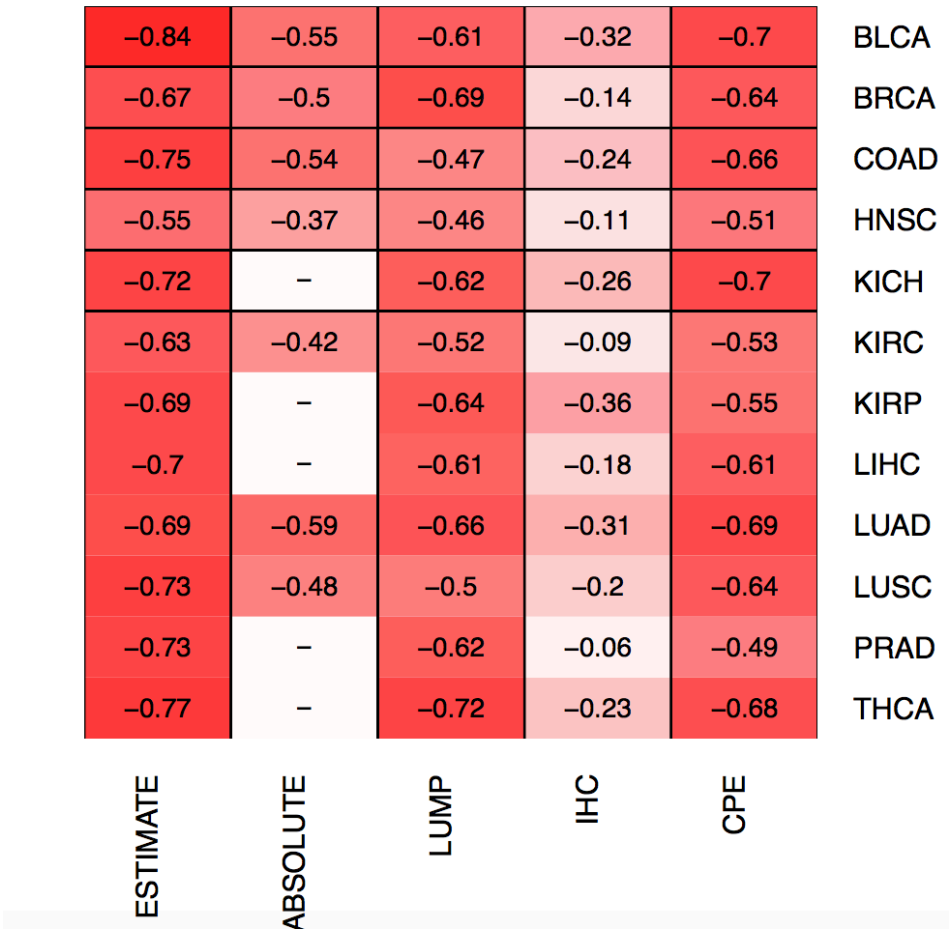
−0.84 −0.55 −0.61 −0.32 −0.7 BLCA
−0.67 −0.5 −0.69 −0.14 −0.64 BRCA
−0.75 −0.54 −0.47 −0.24 −0.66 COAD
−0.55 −0.37 −0.46 −0.11 −0.51 HNSC
−0.72 − −0.62 −0.26 −0.7 KICH
−0.63 −0.42 −0.52 −0.09 −0.53 KIRC
−0.69 − −0.64 −0.36 −0.55 KIRP
−0.7 − −0.61 −0.18 −0.61 LIHC
−0.69 −0.59 −0.66 −0.31 −0.69 LUAD
−0.73 −0.48 −0.5 −0.2 −0.64 LUSC
−0.73 − −0.62 −0.06 −0.49 PRAD
−0.77 − −0.72 −0.23 −0.68 THCA
ESTIMATE
ABSOLUTE
LUMP
IHC
CPE

Figure S4: Correlations between the endogenous superoxide genes and the predicted level of cytosolic Fenton reaction as well as between the mitochondrial superoxide genes and the level of cytosolic Fenton reaction across the 14 cancer types. The expressions of NOX1 and NOX4 are used to reflect the level of superoxide from the endogenous source; the expression of SOD2 is used to reflect the level of mitochondrial superoxide; and expressions of proteasome genes PSMA7 and PSMB4 are used to reflect the level of cytosolic Fenton reactions. The first CC represents the correlation coefficient between a gene and PSMA7 and the second CC represents the correlation coefficient between a gene and PSMB4. CC in bold represents that Fenton reactions rely more on the corresponding source of superoxide.

BLCA	**control**	**stage 1**	**stage 2**	**stage 3**	**stage 4**	**CC**	**CC**
PSMA7	72.9112271	72.0763063	124.030175	129.401674	131.810479		
PSMB4	78.8621046	80.534106	153.733492	145.892057	140.93379		
NOX1	0.73958377	0.74100404	1.76709117	1.56171742	1.18152572	**0.85161712**	**0.93941809**
NOX4	0.32328864	0.37479436	0.40940927	0.69007096	0.6400091	**0.80972631**	**0.69145229**
SOD2	29.7088413	34.9794644	16.3114703	21.2795546	16.1300709	-0.9372753	-0.935444
BRCA							
PSMA7	55.9356972	85.6213178	97.6023441	100.600975	154.190218		
PSMB4	65.0905132	113.464754	126.034573	121.707803	131.508006		
NOX1	0.26367301	0.47546311	0.53290257	0.50864712	0.53904338	**0.76967722**	**0.99838893**
NOX4	1.49584993	1.75881854	1.74515994	1.93591409	1.88598829	**0.7656768**	**0.89311034**
SOD2	27.4430744	15.9551452	18.4304402	13.9331337	10.9971218	-0.8658471	-0.9192173
COAD							
PSMA7	77.3071572	197.347516	196.219826	205.25944	209.138067		
PSMB4	74.2711288	108.80792	114.137064	111.825726	113.947837		
NOX1	42.0482333	88.0252221	80.0340998	72.2849617	81.4725762	**0.93349295**	**0.92572482**
NOX4	0.04652974	0.43589246	0.44320006	0.55527694	0.48859464	**0.98297511**	**0.96839388**
SOD2	16.6770675	20.7736572	20.3334649	19.4792307	17.6287703	0.66529261	0.67458345
ESCA							
PSMA7	23.8940514	83.9392771	87.0372876	96.6155646			
PSMB4	22.9508623	68.6087729	69.5389584	60.5611607			
NOX1	0.09293534	3.36082607	1.74092318	1.52794684		0.704492	0.83488364
NOX4	0.04907046	0.54576441	0.78434954	0.98053157		0.9528037	0.81849838
SOD2	5.73979777	24.2410827	25.9100121	19.973803		**0.91046496**	**0.99493957**

HNSC	control	stage 1	stage 2	stage 3	stage 4	CC	CC
PSMA7	77.6375331	113.602266	124.599011	143.172375	133.139062		
PSMB4	62.248678	87.8673266	103.678942	118.636587	107.48111		
NOX1	0.32911777	0.26289654	0.30770326	0.33864801	0.31804468	0.08755525	0.17928588
NOX4	0.21387194	0.82221947	0.82546344	0.77090906	1.03668439	**0.85812591**	**0.81174379**
SOD2	38.964377	27.4850516	32.120995	31.220703	32.26972	-0.6608189	-0.5851135
KICH							
PSMA7	76.1450489	88.8548807	96.6350418	88.8104462	106.691658		
PSMB4	91.0170463	60.5530052	63.0836777	61.5910723	90.057971		
NOX1	0.29341745	0.23721221	0.23124951	0.19375698	0.26704625	-0.1886554	**0.86595068**
NOX4	7.7396487	4.04611144	4.54284191	4.42933441	2.92534898	-0.8895381	**0.32792244**
SOD2	34.1194907	21.8496659	17.7432578	23.8072583	24.3224544	-0.6486217	**0.72987078**
KIRC							
PSMA7	55.032104	58.3181604	65.6903182	58.3308178	67.7303697		
PSMB4	65.5305596	77.1156681	86.376151	86.185863	95.3937618		
NOX1	0.30949554	0.27728992	0.33402987	0.3175669	0.33429947	0.68313203	0.59291569
NOX4	13.9417762	5.80512464	6.23619497	5.81148985	5.71675277	-0.6061104	-0.8238172
SOD2	39.5275792	79.0383144	84.9739531	99.9381393	110.423609	**0.71222552**	**0.96316464**
KIRP							
PSMA7	62.6753434	74.6593276	80.9586978	86.0521676	76.9729025		
PSMB4	75.3117031	86.308255	82.714043	103.09291	101.326702		
NOX1	0.2860416	0.44712792	0.36777868	0.41465954	0.48043707	0.57506792	0.77663458
NOX4	17.9188256	6.59059043	6.29203674	5.46691126	3.78969729	-0.8529794	-0.7671085
SOD2	30.8744613	59.6591469	85.4972044	74.8952512	71.9019373	**0.91453404**	**0.57232036**

LICH	control	stage 1	stage 2	stage 3	stage 4	CC	CC
PSMA7	51.3480517	86.3683704	98.0891079	102.288723	105.141248		
PSMB4	53.7176745	132.135302	164.357027	139.388194	153.184184		
NOX1	0.14641839	0.29713912	0.62405587	0.44580437	0.32525315	**0.71128873**	**0.81108197**
NOX4	0.02163655	0.22867119	0.25743931	0.24287408	0.18121293	**0.87085266**	**0.92126172**
SOD2	41.5598906	41.7369159	46.6887173	36.8126768	47.8484294	0.22192871	0.37073121
LUAD							
PSMA7	70.2135569	101.513521	105.732898	99.4624108	99.8986679		
PSMB4	58.610936	118.813878	123.941241	122.748355	116.715206		
NOX1	0.3020541	0.97170477	0.83734872	0.93023829	0.62789986	**0.87220313**	**0.89665912**
NOX4	0.34412088	0.92233904	0.94539201	0.9061349	0.75089191	**0.96825606**	**0.97253492**
SOD2	31.1992096	25.0699011	24.764862	26.938668	29.928151	-0.7752152	-0.7463703
LUSC							
PSMA7	71.7567967	130.205469	125.706652	137.823866	162.548458		
PSMB4	61.7792597	130.329259	128.943894	143.040557	134.60966		
NOX1	0.25793753	0.46888267	0.49831254	0.41030714	0.28594148	0.2709081	0.59371158
NOX4	0.40363394	1.08010394	1.12978626	1.04227061	1.66640538	**0.96508655**	**0.80597641**
SOD2	44.7271035	27.4121053	30.1292077	26.3525742	20.4395935	-0.9969738	-0.9297139
PRAD							
PSMA7	80.6802567	81.5233133	84.9913901	80.7463778	70.552348		
PSMB4	80.9576769	88.7512372	87.3161345	90.2318497	77.2898126		
NOX1	0.26988774	0.78052576	1.54159019	0.55231348	0.26289995	**0.70348128**	**0.56384138**
NOX4	2.14841598	1.38320943	2.15735371	2.26998858	2.63947237	-0.5770133	-0.5935374
SOD2	56.390662	15.0642666	24.4954347	17.7156829	16.3309119	0.21722551	-0.3539088

STAD	control	stage 1	stage 2	stage 3	stage 4	CC	CC
PSMA7	57.6124503	102.445457	92.7758302	96.9205256	106.405614		
PSMB4	50.357211	78.2542704	73.6589431	66.6710069	74.2827847		
NOX1	0.18594045	3.30501591	4.24304864	6.16109739	4.4023152	0.81161689	0.64144637
NOX4	0.16188633	0.43426178	0.67911102	0.62285286	0.62761381	0.81398039	0.73534731
SOD2	9.97023722	21.3981888	18.230011	19.606066	18.2194614	**0.93535049**	**0.92009462**
THCA							
PSMA7	57.6217934	63.5507263	64.1110411	65.1140187	61.6960437		
PSMB4	75.0501805	83.8875104	83.0187821	89.7197061	87.5974996		
NOX1	0.26055488	0.47803604	0.41797077	0.45897843	0.48535405	**0.80498554**	**0.89867137**
NOX4	0.21653687	1.10203469	0.93076473	1.39230639	1.32477374	**0.82198515**	**0.98780453**
SOD2	10.5927377	10.4241546	9.11470123	10.5605152	9.47555875	-0.242064	-0.2025304

Figure S5: Increased accumulation of cytosolic Fe^{3+} in 14 cancer types. Here we use the expressions of FTL in control tissues vs cancer tissues from stage 1 through stage 4 to reflect the increase in the cytosolic Fe^{3+} accumulation. Rows highlighted in red represent cancer types with reduced Fe^{3+} accumulation as reflected by FTL.

Cancer	Gene	Normal	Stage 1	Stage 2	Stage 3	Stage 4
BLCA	FTL	2665.772811	1796.45979	2565.189782	3521.479845	3479.735276
BRCA	FTL	2596.076577	1924.098137	2058.495214	2269.136435	2360.502725
COAD	FTL	2447.157783	2838.531429	3074.708221	3026.259628	2904.17878
ESCA	FTL	1388.955785	2060.922253	3503.258922	2432.133226	
HNSC	FTL	954.8875571	1421.954244	1980.993255	2002.137894	2168.805584
KICH	FTL	3170.52011	2258.704081	2177.821507	2967.037043	3616.675187
KIRC	FTL	3333.129485	3423.591223	3487.658951	3980.241959	4033.165465
KIRP	FTL	4576.165659	5624.951794	8886.72965	6620.562354	5921.977015
LICH	FTL	6020.631537	12355.49985	14109.94635	10092.13708	19946.81214
LUAD	FTL	7583.141208	5413.562625	5232.977912	4742.051967	4973.764998
LUSC	FTL	7591.464488	5227.002192	4590.880108	5820.370444	5070.442008
PFRAD	FTL	5152.808273	2538.156425	3301.714459	3518.67506	3951.575325
STAD	FTL	2107.785591	2866.972766	3077.818732	3054.121857	2821.790252
THCA	FTL	1971.517442	1915.949388	1755.770734	2049.366082	1824.36838

Figure S6: Negative correlation between estimated Fe^{3+} accumulation and H^{+} exporter genes across the 14 cancer types. (PSMA7, PSMB4), and (FTH1, FTL) are used to represent the level of Fenton reactions and the accumulation of Fe^{3+}. And all the SLC genes used here are acid-extruding transporters.

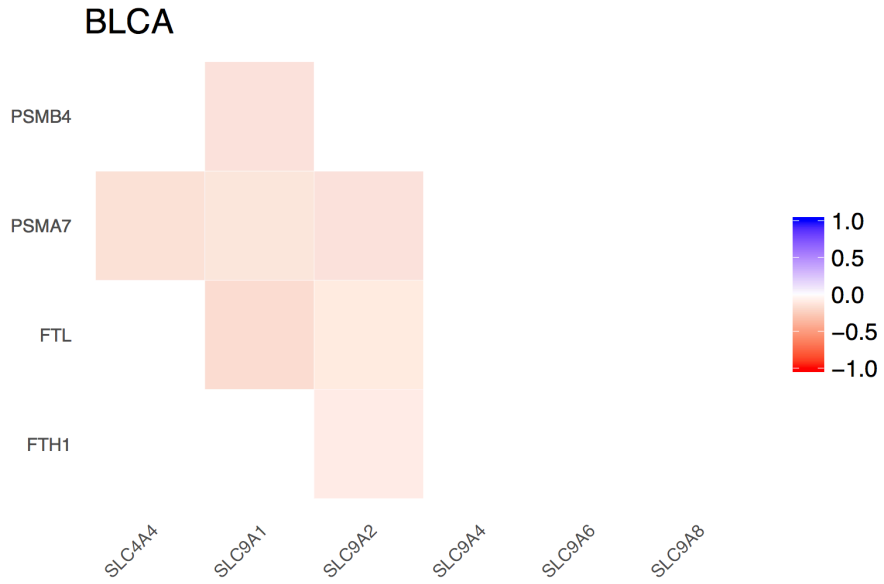

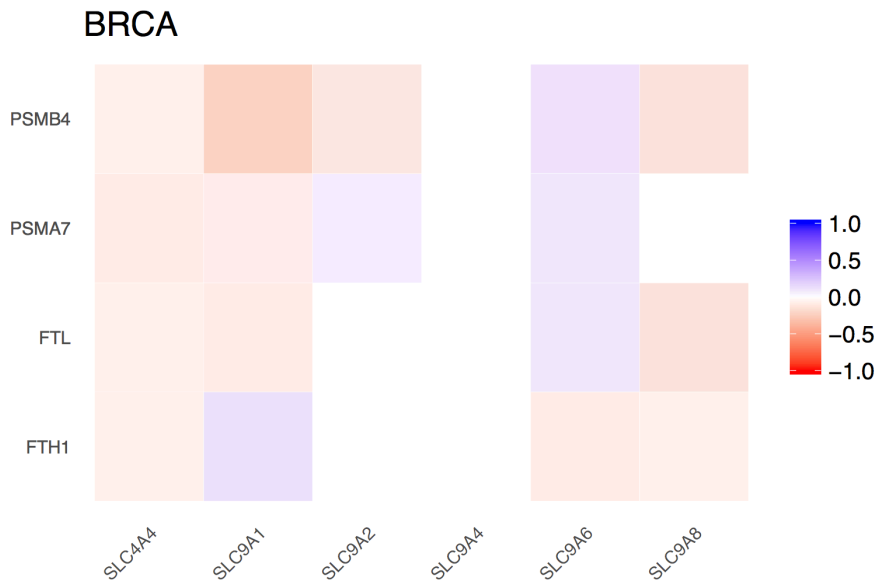

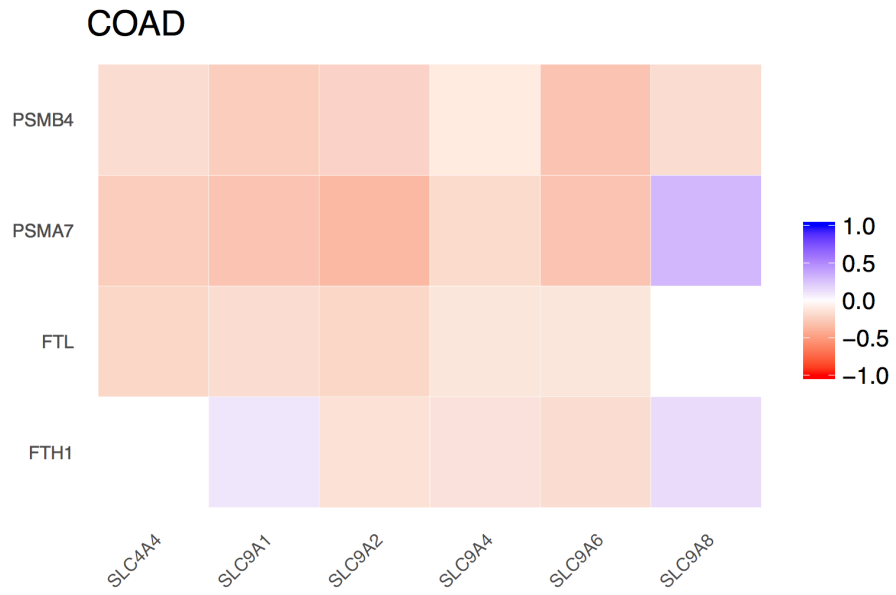
COAD
PSMB4
PSMA7
FTL
FTH1
SLC4A4
SLC9A1
SLC9A2
SLC9A4
SLC9A6
SLC9A8
1.0
0.5
0.0
−0.5
−1.0

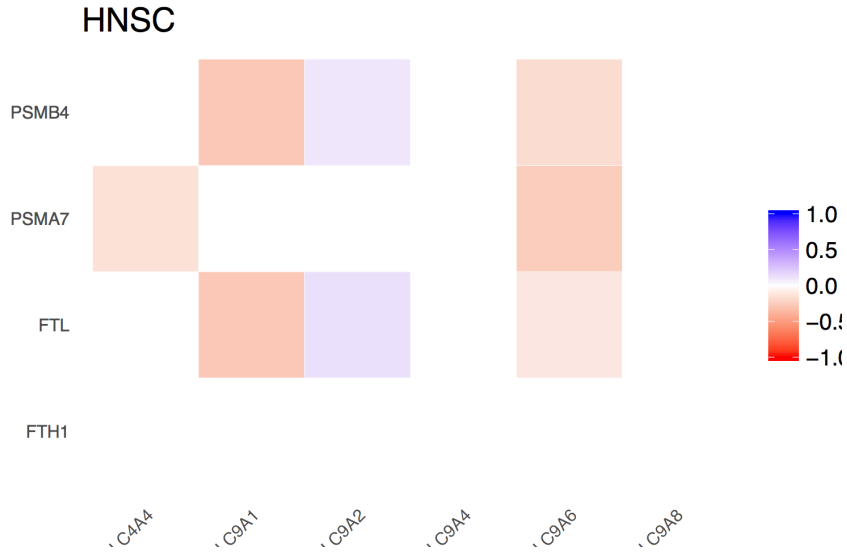
HNSC
PSMB4
PSMA7
FTL
FTH1
1.0
0.5
0.0

KICH

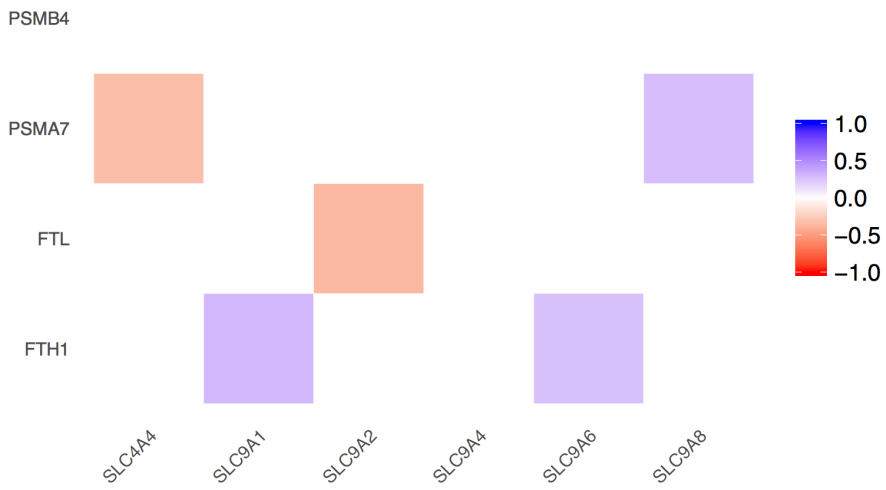
PSMB4
PSMA7
FTL
FTH1
SLC4A4
SLC9A1
SLC9A2
SLC9A4
SLC9A6
SLC9A8
1.0
0.5
0.0
−0.5
−1.0

KIRC

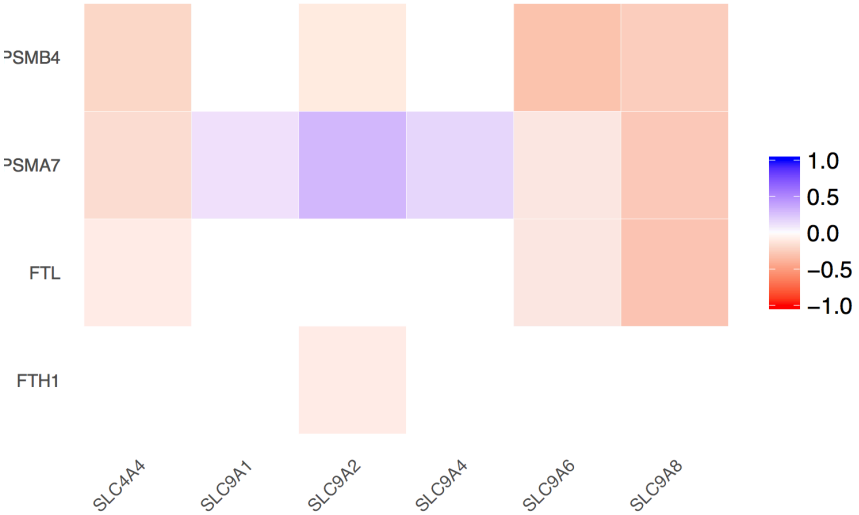
PSMB4
PSMA7
FTL
FTH1
SLC4A4
SLC9A1
SLC9A2
SLC9A4
SLC9A6
SLC9A8
1.0
0.5
0.0
−0.5
−1.0

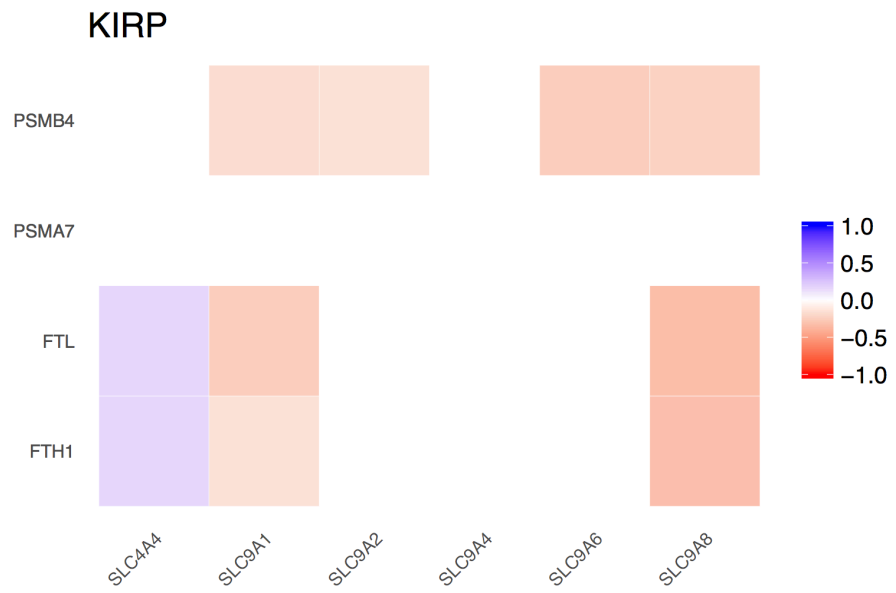
KIRP
PSMB4
PSMA7
FTL
FTH1
SLC4A4
SLC9A1
SLC9A2
SLC9A4
SLC9A6
SLC9A8
1.0
0.5
0.0
−0.5
−1.0

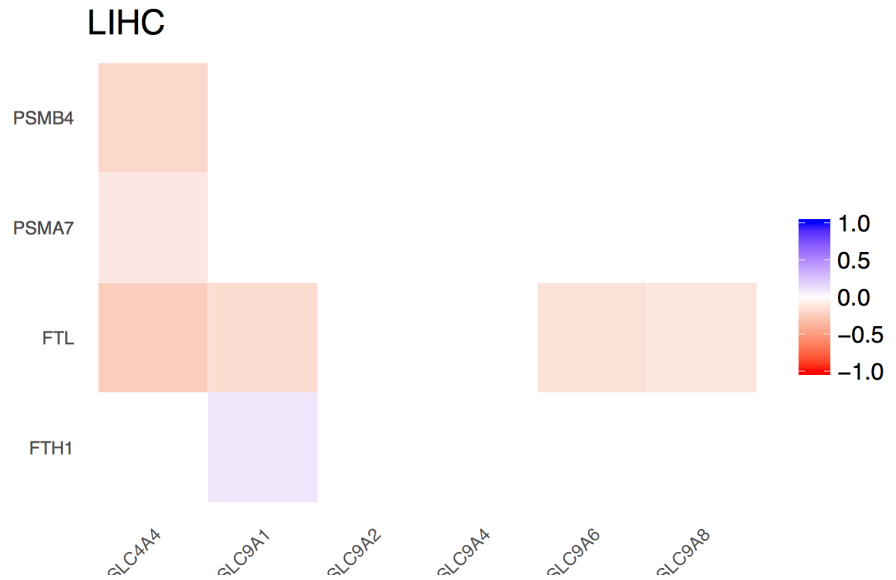
LIHC
PSMB4
PSMA7
FTL
FTH1
SLC4A4
SLC9A1
SLC9A2
SLC9A4
SLC9A6
SLC9A8
1.0
0.5
0.0
−0.5
−1.0

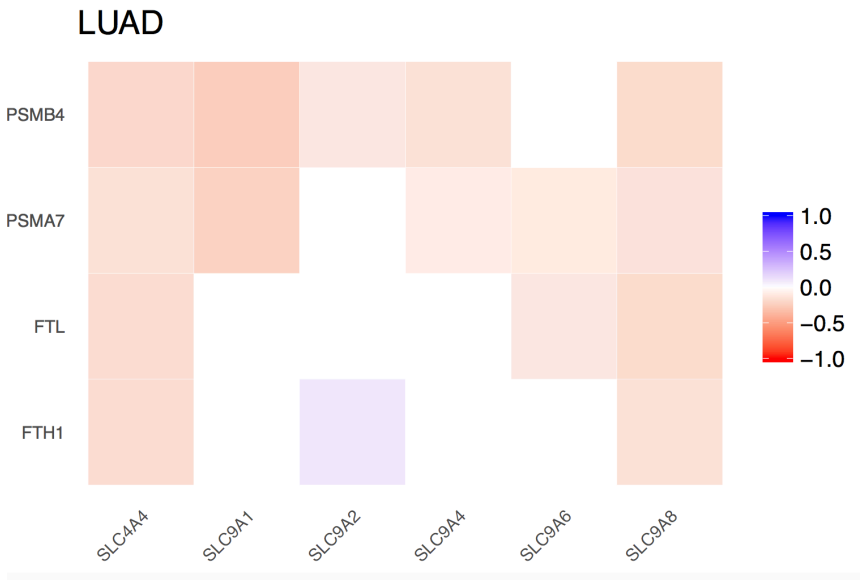
LUAD
PSMB4
PSMA7
FTL
FTH1
SLC4A4
SLC9A1
SLC9A2
SLC9A4
SLC9A6
SLC9A8
1.0
0.5
0.0
−0.5
−1.0

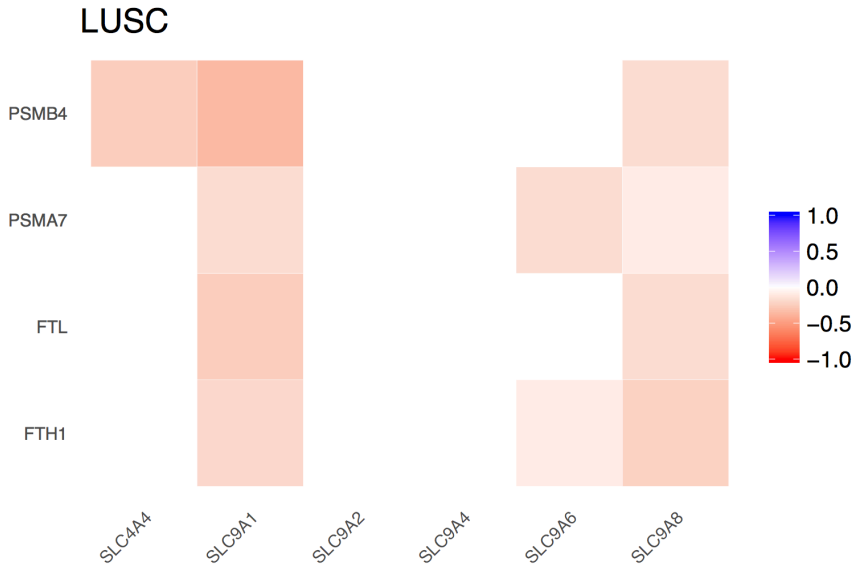
LUSC
PSMB4
PSMA7
FTL
FTH1
SLC4A4
SLC9A1
SLC9A2
SLC9A4
SLC9A6
SLC9A8
1.0
0.5
0.0
−0.5
−1.0

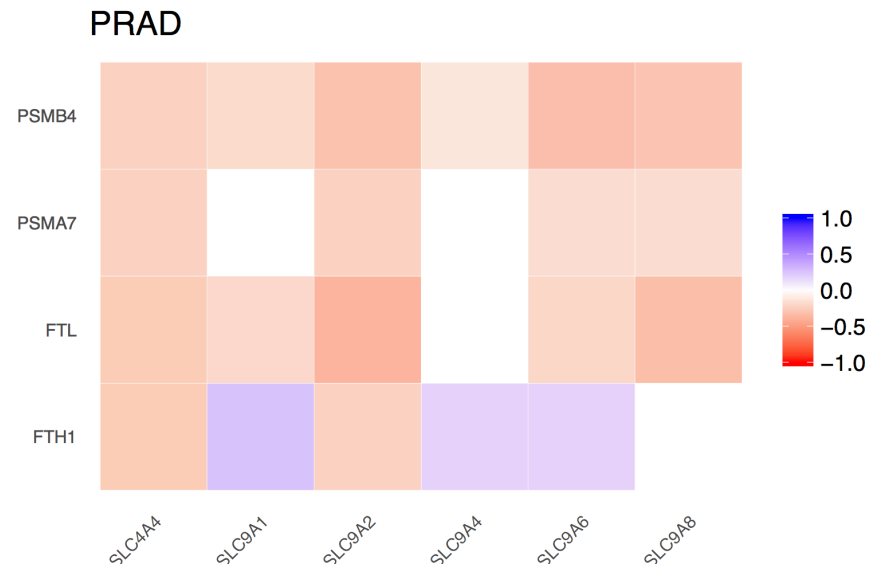
PRAD
PSMB4
PSMA7
FTL
FTH1
SLC4A4
SLC9A1
SLC9A2
SLC9A4
SLC9A6
SLC9A8
1.0
0.5
0.0
−0.5
−1.0

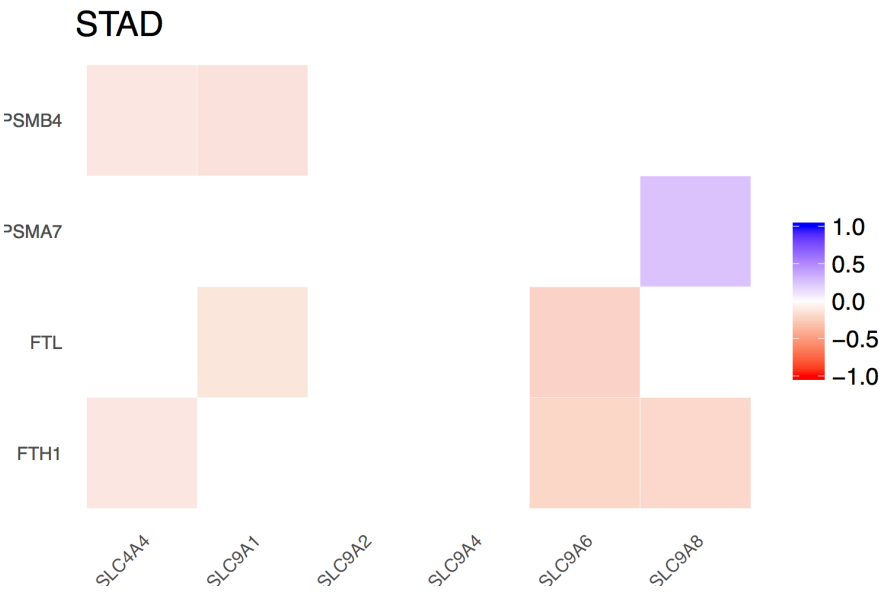
STAD
PSMB4
PSMA7
FTL
FTH1
SLC4A4
SLC9A1
SLC9A2
SLC9A4
SLC9A6
SLC9A8
1.0
0.5
0.0
−0.5
−1.0

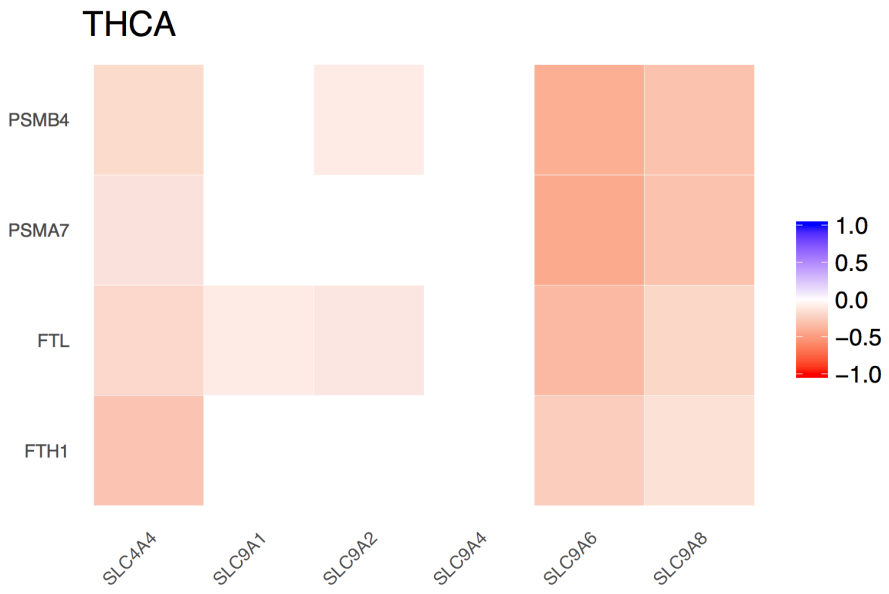
THCA
PSMB4
PSMA7
FTL
FTH1
SLC4A4
SLC9A1
SLC9A2
SLC9A4
SLC9A6
SLC9A8
1.0
0.5
0.0
−0.5
−1.0

Figure S7: Correlations between the expressions of acid-loading and acid-extruding transporter genes and the predicted level of cytosolic Fenton reactions as well as with OH^--producing cytosolic Fenton reactions. 65 protein damage-responsive genes are selected to be regressed with the Fenton reaction related genes linked via the Michaelis-Menten equation for predicting the occurrence of Fenton reactions. In each panel, the bar on the left shows the correlations between the expressions of selected acid-loading and acid-extruding transporter genes and the level of OH^--producing cytosolic Fenton reactions predicted by the 65 genes while the bar on the right shows the correlation between these transporter genes and the predicted cytosolic Fenton reaction level. The names of the acid-loading and acid-extruding transporter genes, the cancer type and the p-value of the difference between the correlations tested by Mann-Whitney test are listed above each box-plot.

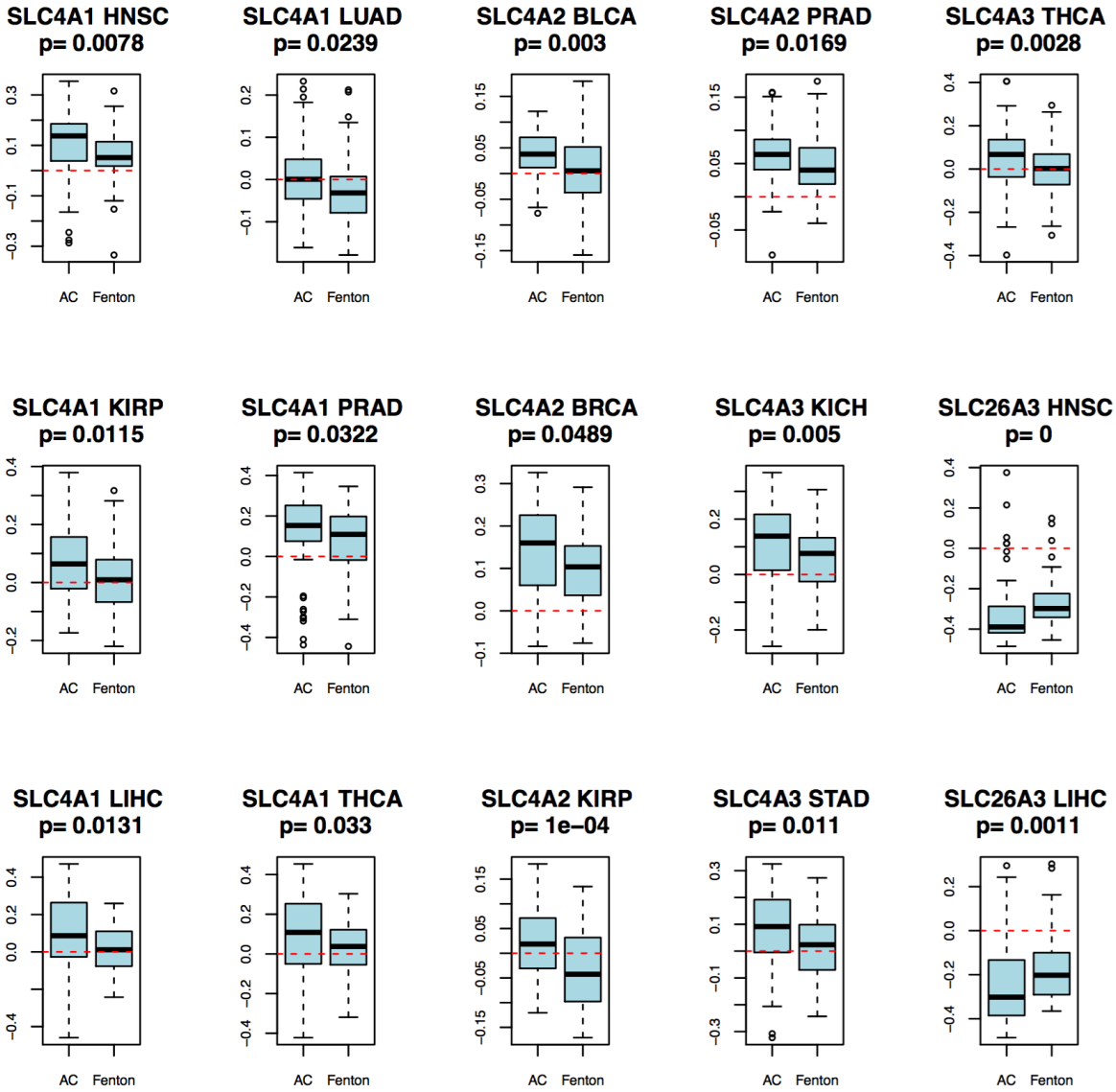
SLC4A1 HNSC
p= 0.0078
SLC4A1 LUAD
p= 0.0239
SLC4A2 BLCA
p= 0.003
SLC4A2 PRAD
p= 0.0169
SLC4A3 THCA
p= 0.0028
SLC4A1 KIRP
p= 0.0115
SLC4A1 PRAD
p= 0.0322
SLC4A2 BRCA
p= 0.0489
SLC4A3 KICH
p= 0.005
SLC26A3 HNSC
p= 0
SLC4A1 LIHC
p= 0.0131
SLC4A1 THCA
p= 0.033
SLC4A2 KIRP
p= 1e−04
SLC4A3 STAD
p= 0.011
SLC26A3 LIHC
p= 0.0011
AC
Fenton

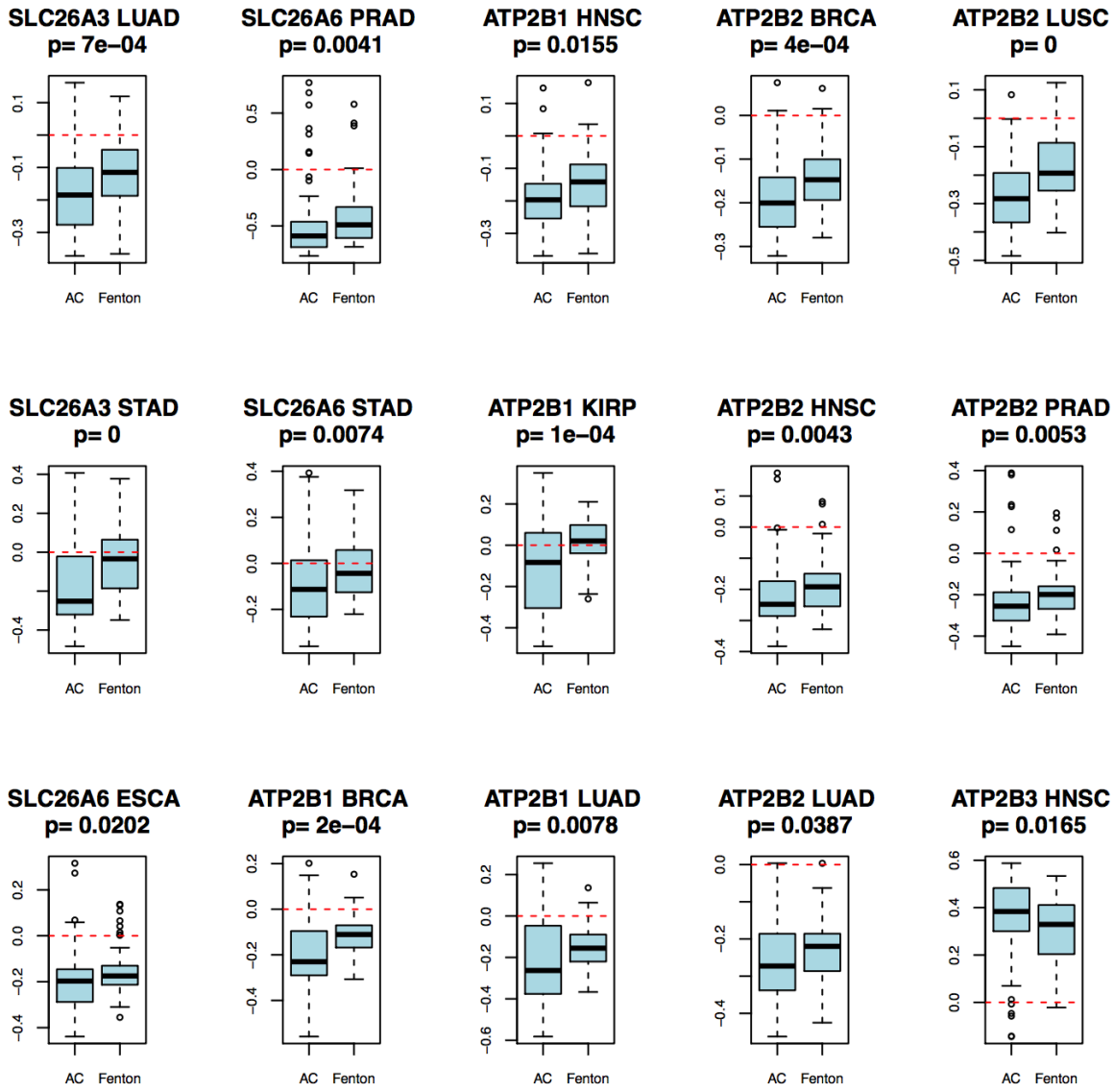
SLC26A3 LUAD
p= 7e−04
SLC26A6 PRAD
p= 0.0041
ATP2B1 HNSC
p= 0.0155
ATP2B2 BRCA
p= 4e−04
ATP2B2 LUSC
p= 0
SLC26A3 STAD
p= 0
SLC26A6 STAD
p= 0.0074
ATP2B1 KIRP
p= 1e−04
ATP2B2 HNSC
p= 0.0043
ATP2B2 PRAD
p= 0.0053
SLC26A6 ESCA
p= 0.0202
ATP2B1 BRCA
p= 2e−04
ATP2B1 LUAD
p= 0.0078
ATP2B2 LUAD
p= 0.0387
ATP2B3 HNSC
p= 0.0165
AC
Fenton

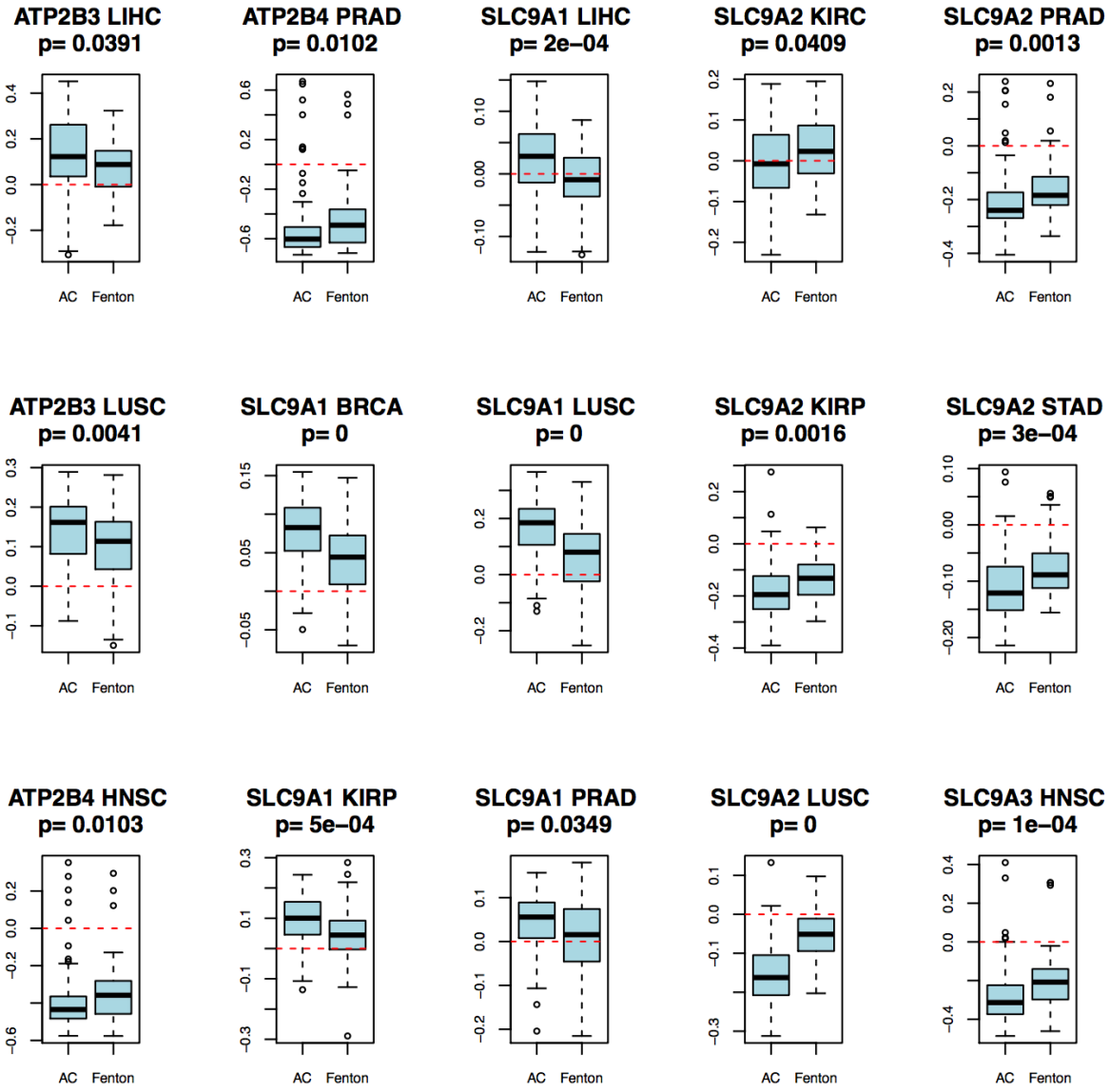
ATP2B3 LIHC
p= 0.0391
ATP2B4 PRAD
p= 0.0102
SLC9A1 LIHC
p= 2e−04
SLC9A2 KIRC
p= 0.0409
SLC9A2 PRAD
p= 0.0013
ATP2B3 LUSC
p= 0.0041
SLC9A1 BRCA
p= 0
SLC9A1 LUSC
p= 0
SLC9A2 KIRP
p= 0.0016
SLC9A2 STAD
p= 3e−04
ATP2B4 HNSC
p= 0.0103
SLC9A1 KIRP
p= 5e−04
SLC9A1 PRAD
p= 0.0349
SLC9A2 LUSC
p= 0
SLC9A3 HNSC
p= 1e−04
AC
Fenton

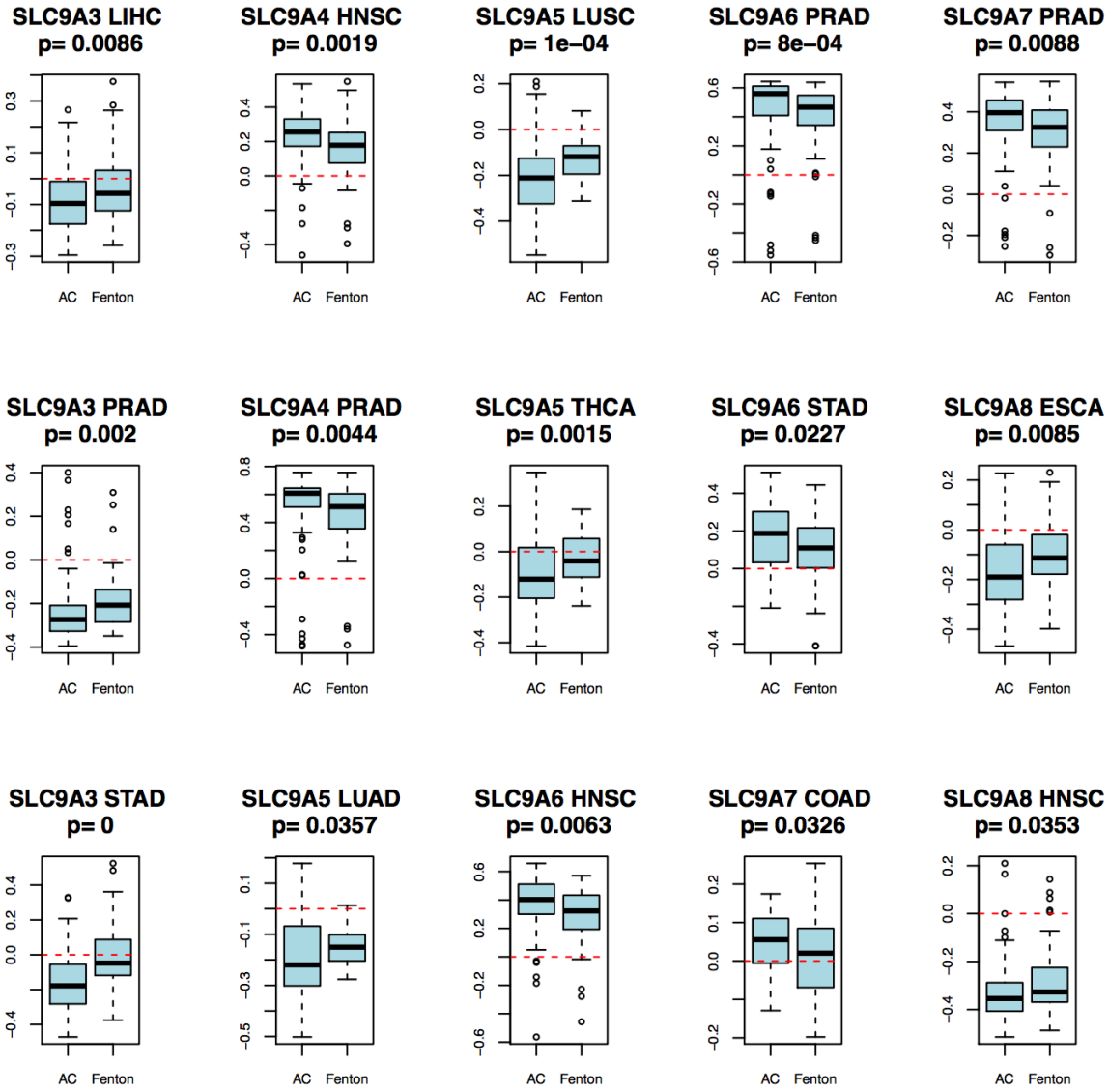
SLC9A3 LIHC
p= 0.0086
SLC9A4 HNSC
p= 0.0019
SLC9A5 LUSC
p= 1e−04
SLC9A6 PRAD
p= 8e−04
SLC9A7 PRAD
p= 0.0088
SLC9A3 PRAD
p= 0.002
SLC9A4 PRAD
p= 0.0044
SLC9A5 THCA
p= 0.0015
SLC9A6 STAD
p= 0.0227
SLC9A8 ESCA
p= 0.0085
SLC9A3 STAD
p= 0
SLC9A5 LUAD
p= 0.0357
SLC9A6 HNSC
p= 0.0063
SLC9A7 COAD
p= 0.0326
SLC9A8 HNSC
p= 0.0353
AC
Fenton

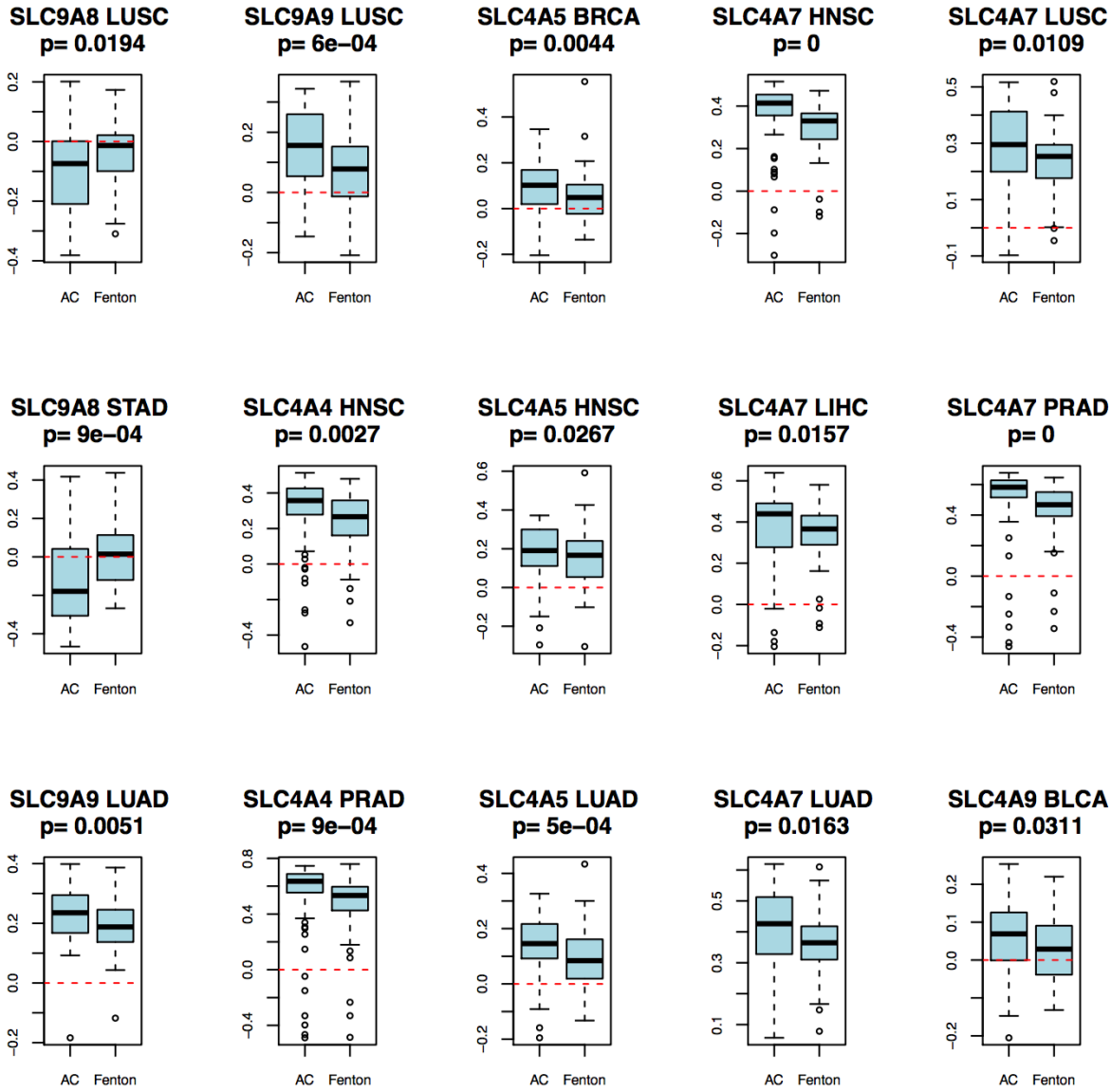
SLC9A8 LUSC
p= 0.0194
SLC9A9 LUSC
p= 6e−04
SLC4A5 BRCA
p= 0.0044
SLC4A7 HNSC
p= 0
SLC4A7 LUSC
p= 0.0109
SLC9A8 STAD
p= 9e−04
SLC4A4 HNSC
p= 0.0027
SLC4A5 HNSC
p= 0.0267
SLC4A7 LIHC
p= 0.0157
SLC4A7 PRAD
p= 0
SLC9A9 LUAD
p= 0.0051
SLC4A4 PRAD
p= 9e−04
SLC4A5 LUAD
p= 5e−04
SLC4A7 LUAD
p= 0.0163
SLC4A9 BLCA
p= 0.0311
AC
Fenton

SLC4A9 BRCA
p= 6e−04

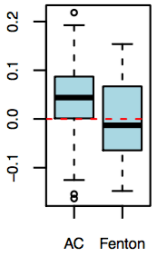

SLC4A9 LUSC
p= 1e−04

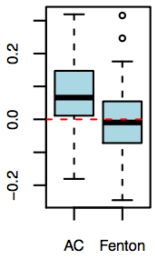

SLC4A9 PRAD
p= 0.0026

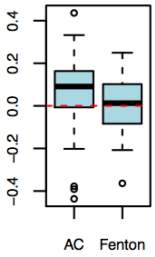

Figure S8: The pyruvate metabolism with the name in each box represents a metabolite and the name next to each edge is the name of the enzyme catalyzing the corresponding reaction.

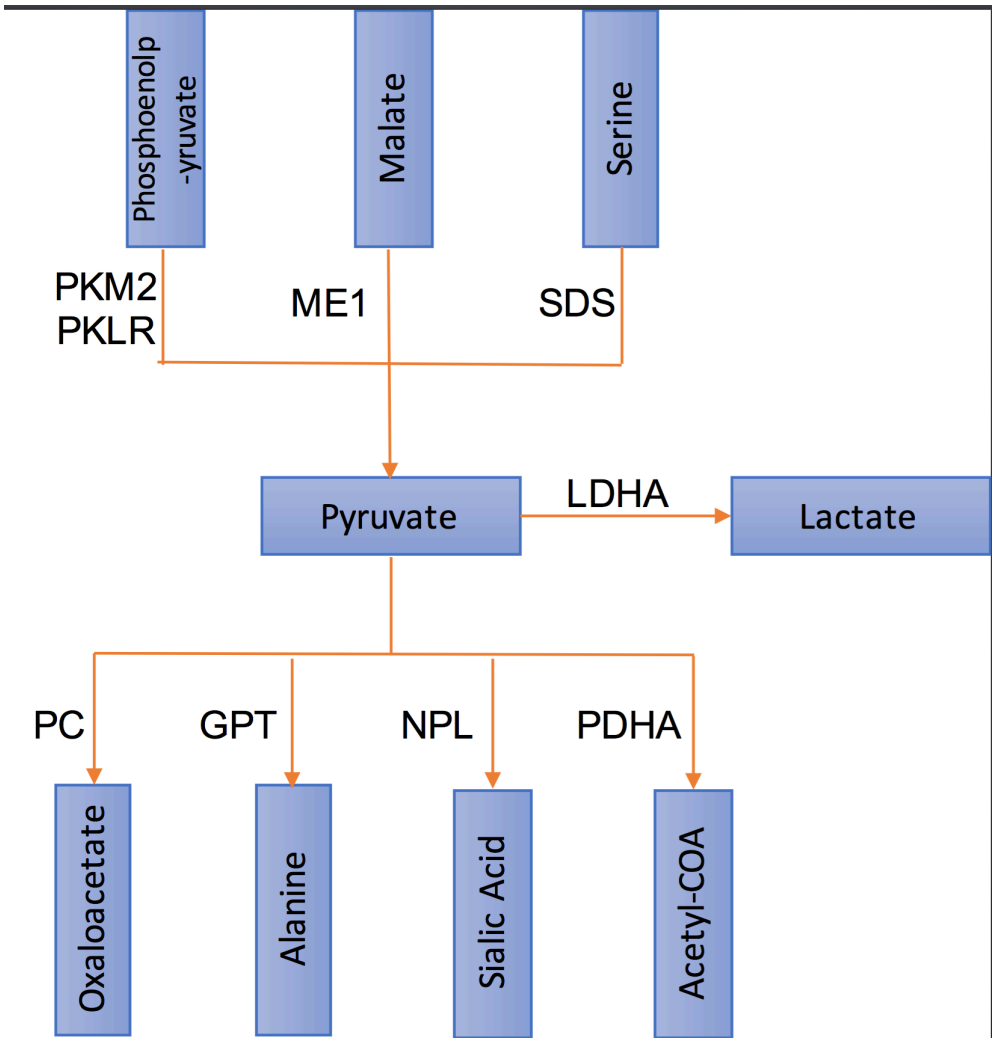

Figure S9: Correlation between the estimated rate of OH^- production and the rate of glycolytic ATP synthesis across 14 cancer types. We used a simpler way to estimate the rate of OH^- production, specifically using the expressions of ferritin gene FTH1 to represent the accumulation rate of unreduced Fe^{3+}; proteasome gene PSMA7 to represent the level of cytosolic Fenton reaction; and PKM to represent the level of glycolytic ATP synthesis. For each cancer type, the three values are: the coefficients a_1 and a_2 of FTH1 and PSMA7, plus the correlation coefficient (CC) between PMK and (a_1* FTH1 + a_2 * PSMA7).

Cancer type	a_1	a_2	CC
BLCA	6.21	12.71	0.3335565
BRCA	10.31	16.41	0.3726417
COAD	1	0	0.102479
ESCA	13.81	19.31	0.273338
HNSC	2.01	10.41	0.2401589
KICH	16.61	19.91	0.4488197
KIRC	11.81	11.71	0.3422485
KIRP	8.91	5.51	0.2605148
LICH	15.31	17.21	0.391865
LUAD	13.81	13.71	0.3588394
LUSC	14.11	10.91	0.319393
PRAD	18.21	10.81	0.5821504
STAD	10.91	10.71	0.3038045
THCA	4.61	5.91	0.4735309

Figure S10: Correlation between glycolysis and aminoacyl-tRNA synthesis, purine synthesis, base excision repair and the glyoxylate and dicarboxylate metabolism, respectively, across six chronical inflammatory diseases. In this plot, PKM is used to reflect the level of glycolytic ATP production, and genes in the four sections along with y-axis, separated by blank lines, are for aminoacyl-tRNA synthesis, purine synthesis, base excision repair and the glyoxylate and dicarboxylate metabolism, respectively. The six disease names to the left of the vertical blank line are six diseases mentioned.

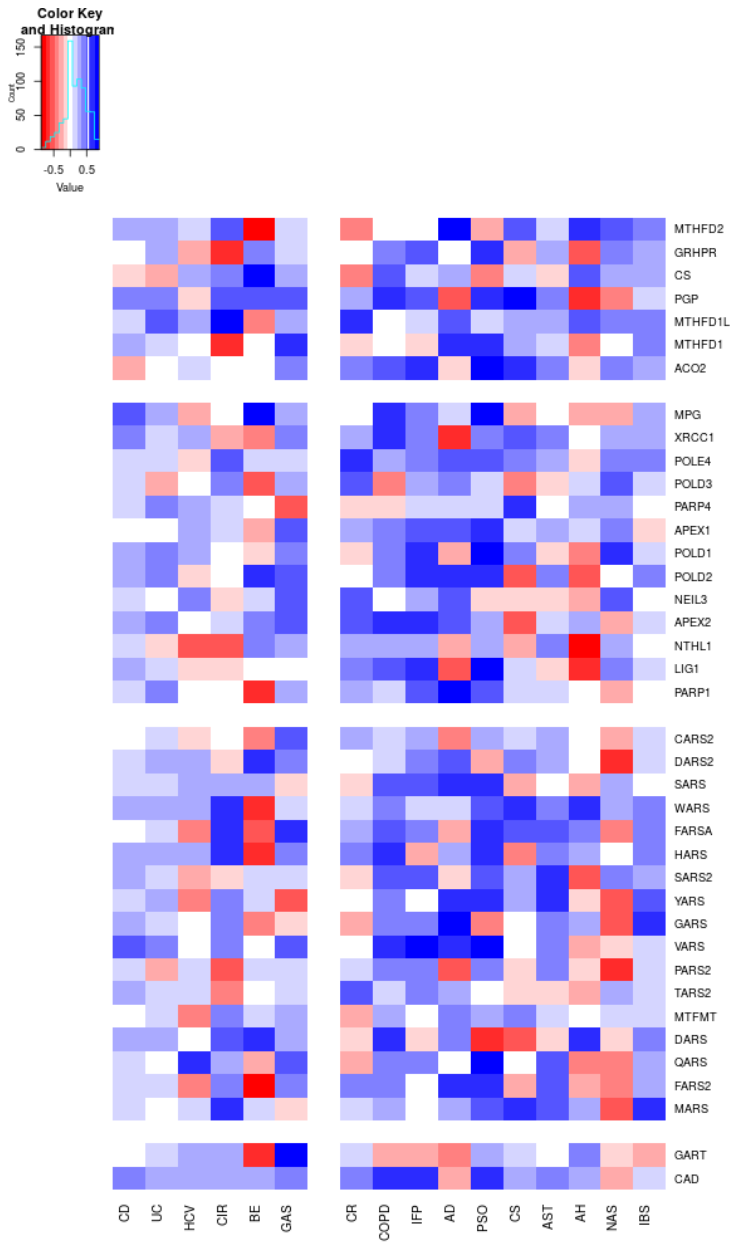

Figure S11: Contribution to mitochondrial Fenton reaction by mitochondrial NADH and superoxide across the 14 cancer types. We use anti-oxidation genes GPX4 and TXN to represent the level of mitochondrial superoxide, MDH1 and MDH2 to reflect the level of mitochondrial NADH level; and CLPP and CLPX to represent the level of mitochondrial Fenton reactions. CC1 represents the correlation coefficient between CLPP and the corresponding gene (on the same row); and CC2 represents the correlation coefficient between CLPX and the corresponding gene. CC values in bold represent strongly correlated mitochondrial Fenton reactions and the relevant NDAH and/or mitochondrial superoxide.

BLCA	**Control**	**Stage 1**	**Stage 2**	**Stage 3**	**Stage 4**	**CC1**	**CC2**
CLPP	14.9429158	16.3176297	25.8732004	24.5908508	23.7649566		
CLPX	7.63452016	11.2240777	9.31985052	8.43213057	8.96137259		
MDH1	26.9327563	25.2657586	28.3644584	27.8921952	29.0741867	**0.79824397**	-0.5325603
MDH2	51.1347134	93.5482608	65.4990539	66.9083649	67.2664207	-0.1158075	**0.96391185**
GPX4	87.4913932	167.259421	120.151081	116.87599	114.982625	-0.0845794	**0.97746829**
TXN	156.573165	124.644194	221.893624	249.039718	217.775072	**0.91126942**	-0.4587534
BRCA							
CLPP	11.3008378	18.2197539	19.7512322	19.9809503	22.350035		
CLPX	10.50458	9.73710224	9.57335914	9.37759076	8.20379345		
MDH1	36.6348765	25.3766674	27.7486895	25.5094688	26.8235312	-0.8834487	**0.63448755**
MDH2	42.2528711	58.9749673	61.5278973	62.8472686	72.2287177	**0.98955246**	-0.9439552
GPX4	151.010186	122.445536	125.822009	136.456964	149.855339	-0.2796073	-0.1543284
TXN	83.2476611	146.395762	162.948839	159.412863	157.816197	**0.95418636**	-0.711995
COAD							
CLPP	20.2195465	34.6559018	35.3426464	32.0970765	33.79039		
CLPX	8.17104139	10.0520693	9.63570544	9.07067961	8.86229873		
MDH1	34.0366323	26.7110388	29.3460265	26.2286669	25.399032	-0.83588	-0.5457289
MDH2	84.4832393	117.642672	115.945689	116.701901	121.589402	**0.96752056**	**0.703781**
GPX4	59.0055601	90.7149836	97.5259952	92.548176	100.38102	**0.96446902**	**0.65288412**
TXN	234.823139	278.530542	309.842033	279.443799	296.816172	**0.92491562**	**0.64055962**
ESCA							
CLPP	10.749054	14.9594702	16.9599272	14.7301429			
CLPX	5.16853734	9.16259986	8.78284076	10.1419215			
MDH1	23.7088776	18.4608795	18.6457598	22.0844009		-0.8413109	-0.5789501
MDH2	31.5189318	65.0436184	67.5009548	59.5330178		**0.96575956**	**0.89217422**
GPX4	39.9606628	74.224511	103.800556	82.2518606		**0.98392495**	**0.78813128**
TXN	49.9179496	262.23977	384.945956	202.073383		**0.97750748**	**0.67783063**

HNSC	Control	Stage 1	Stage 2	Stage 3	Stage 4	CC1	CC2
CLPP	16.7280953	17.5470792	17.9411458	19.4732531	19.6210513		
CLPX	11.3464565	10.8059705	9.88704378	9.93029715	9.48454317		
MDH1	30.950675	21.9922954	24.7685305	25.2054515	25.4172737	-0.3725843	**0.44434819**
MDH2	80.9172916	62.9219946	63.4820039	69.4617378	69.9175443	-0.2852798	**0.4878081**
GPX4	65.3250484	58.7003959	68.598607	81.8823665	76.1997965	**0.84470482**	-0.702242
TXN	452.199531	357.747308	314.640518	328.449716	344.619937	-0.6774217	**0.83531426**
KICH							
CLPP	23.0940841	18.0491271	22.3595701	19.4135189	22.1255149		
CLPX	11.4274104	10.4126917	9.97279757	8.42390126	11.778824		
MDH1	47.3625442	39.8576725	34.9791536	36.9320537	37.348874	0.26122711	**0.47272871**
MDH2	65.2014185	84.055682	106.412641	102.239609	134.69847	0.08203079	0.03438718
GPX4	131.60401	179.112548	200.58036	182.627694	199.94719	-0.2153407	-0.2424554
TXN	92.8772713	64.4361043	69.0052841	70.8548471	116.052772	**0.60226927**	**0.74322377**
KIRC							
CLPP	16.1195678	19.1990377	19.1441019	19.172136	20.0827161		
CLPX	11.3585288	7.62324305	7.6599199	6.76863962	6.93509859		
MDH1	46.2121237	26.2438366	29.3927105	24.1704258	25.3123965	**-0.9609778**	**0.99243815**
MDH2	59.220296	45.5790645	47.2475993	42.9443734	45.0596997	-0.9424742	**0.99256335**
GPX4	92.5087933	124.582069	136.547542	134.470014	148.847308	**0.96998664**	-0.9393425
TXN	92.3935476	105.642217	110.228278	102.868059	123.439869	**0.86105649**	-0.7277827
KIRP							
CLPP	21.2982236	21.1570013	21.6621797	22.4481916	22.5688467		
CLPX	10.6589035	7.9208945	8.45145883	8.39230535	7.27749264		
MDH1	45.8895284	39.4944526	41.7699467	44.6571765	33.2688813	-0.3974285	**0.80247703**
MDH2	67.2479559	76.1036806	86.0600562	72.0024621	73.9531822	-0.0608682	-0.4601841
GPX4	133.282205	224.88819	207.051719	231.626118	231.793235	**0.55885493**	-0.9504752
TXN	97.6511517	156.351043	144.632248	217.589676	254.209354	**0.89157119**	-0.8108664

LICH	Control	Stage 1	Stage 2	Stage 3	Stage 4	CC1	CC2
CLPP	15.7859742	20.7758792	21.4972598	22.1713368	20.9724764		
CLPX	13.2317026	11.233021	10.5327798	10.397691	12.4007909		
MDH1	20.8540297	31.800815	33.8223921	34.801405	39.6982448	**0.88463013**	-0.5035172
MDH2	46.9342578	77.422197	85.4121924	78.9015099	89.6986644	**0.92008992**	-0.6132537
GPX4	118.535748	185.797023	203.502388	184.040607	225.79777	**0.85195217**	-0.4834505
TXN	102.344458	247.250997	286.8325	277.116803	313.375927	**0.94280978**	-0.6406543
LUAD							
CLPP	13.8302137	16.5399924	16.9845012	17.772196	16.0995941		
CLPX	7.18374051	8.50769602	8.67640931	9.21918705	9.72290474		
MDH1	18.9633082	22.7318224	22.424518	24.2968416	25.1505771	**0.77300332**	**0.99219771**
MDH2	33.241278	57.0462458	61.2997111	66.2300105	70.6379732	**0.83857356**	**0.98324268**
GPX4	95.2232375	131.753779	128.329027	121.885223	136.094873	**0.72781844**	**0.85815372**
TXN	98.9132486	186.350452	177.371116	195.035568	242.238013	**0.68180094**	**0.97753506**
LUSC							
CLPP	13.2586402	19.6151637	20.7949736	21.1168082	17.7402734		
CLPX	7.30633593	9.4535728	9.37342255	9.52077519	7.86379191		
MDH1	18.7293796	37.0852507	37.7125962	41.1386965	44.5308508	**0.79604399**	**0.55430711**
MDH2	34.5661221	75.5987058	75.4706745	77.4514595	78.8385754	**0.89088145**	**0.70979488**
GPX4	95.7047793	103.69478	110.547286	110.25994	110.391303	**0.83157811**	**0.57180802**
TXN	91.0516325	299.507921	303.159604	301.190383	183.629748	**0.97148343**	**0.98568513**
PRAD							
CLPP	15.4292425	20.9744554	16.9942068	15.5747001	14.1279579		
CLPX	8.37788858	7.30699149	7.55165753	6.2833734	6.37299464		
MDH1	21.5961479	21.9431112	19.3257272	18.6480059	19.0226407	**0.62463266**	**0.72688911**
MDH2	39.3564885	55.9512006	50.6323291	47.2396206	44.3930951	**0.84180713**	-0.2183041
GPX4	101.794167	125.235841	95.3077179	91.968044	73.483542	**0.91447001**	**0.49313701**
TXN	87.0460331	145.500768	156.69939	132.362574	129.910083	**0.45256853**	**-0.4503743**

STAD	Control	Stage 1	Stage 2	Stage 3	Stage 4	CC1	CC2
CLPP	19.9202902	19.488149	20.8999006	19.0119308	19.835184		
CLPX	7.28077918	9.03890891	8.62591002	8.98318224	8.82470913		
MDH1	21.6564578	19.7288634	19.1565037	18.0937371	18.5948555	0.23309808	-0.8742238
MDH2	61.9746758	88.9162823	80.109352	74.2353639	86.4341961	0.00665141	**0.84478848**
GPX4	92.6426806	91.5765552	99.3673001	95.265027	105.374352	0.34771409	0.28088202
TXN	217.070571	254.673492	227.360803	213.523705	226.041887	0.02321887	**0.42635944**
THCA							
CLPP	15.4751853	17.3665088	18.3932415	18.4289401	17.5456603		
CLPX	9.0156049	9.96022075	9.90361466	9.92203466	9.33454219		
MDH1	24.1824954	26.7295201	28.5241815	26.4652883	25.9266452	**0.84961754**	**0.82604385**
MDH2	40.3507477	40.0943406	52.7060055	39.8452209	39.2680782	**0.40459469**	0.35527561
GPX4	101.572724	167.799913	162.949971	188.345775	185.460452	**0.87671474**	**0.66602831**
TXN	66.5405764	78.1672272	69.0460641	86.0535223	79.1994823	**0.57748049**	**0.48465627**

Figure S12: (A) Correlations between the predicted level of mitochondrial Fenton reactions and the expressions of ETC Complex I genes in the more hypoxic and less hypoxic samples, respectively; (B) Correlations between the predicted level of mitochondrial Fenton reaction and ETC Complex III genes in the more hypoxic and less hypoxic samples, respectively. Each box-plot shows the correlations between the level of mitochondrial Fenton reaction predicted by the regression model (tilted in each figure) and the expression levels of Complex I (or III) genes in the more hypoxic samples (left bar, H) and less hypoxic samples (right bar, N).

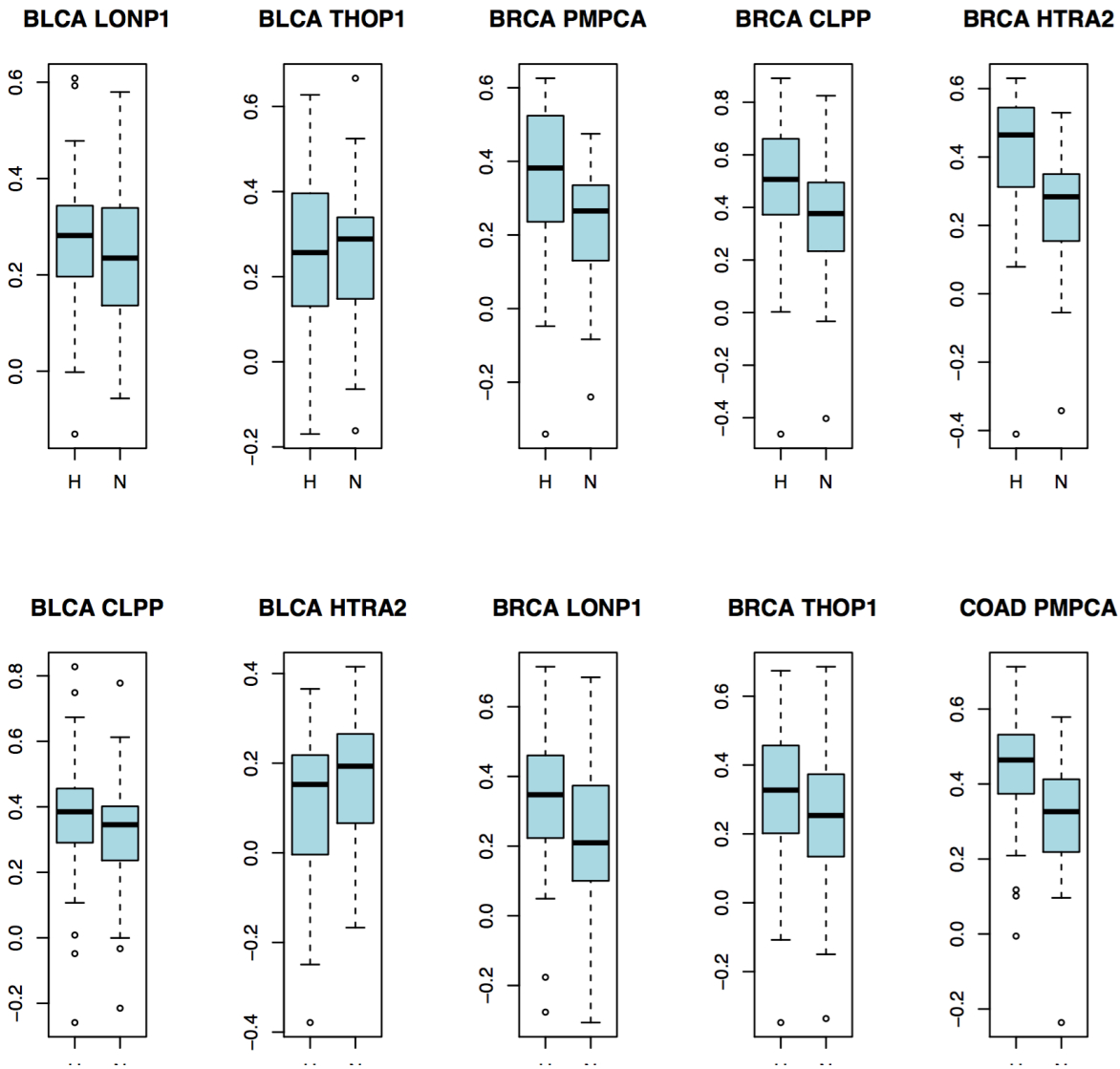

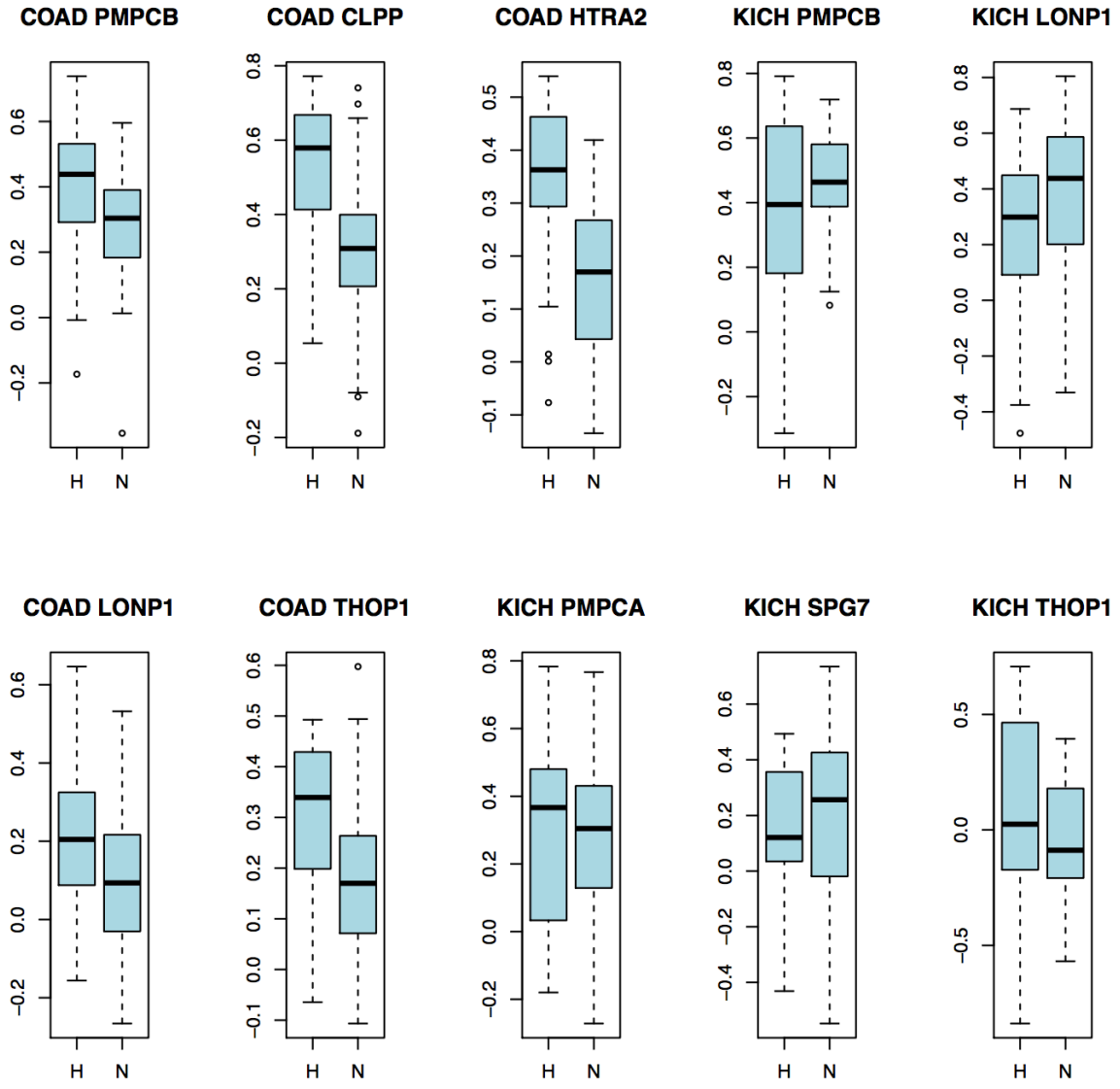
COAD PMPCB
COAD CLPP
COAD HTRA2
KICH PMPCB
KICH LONP1
COAD LONP1
COAD THOP1
KICH PMPCA
KICH SPG7
KICH THOP1
H
N

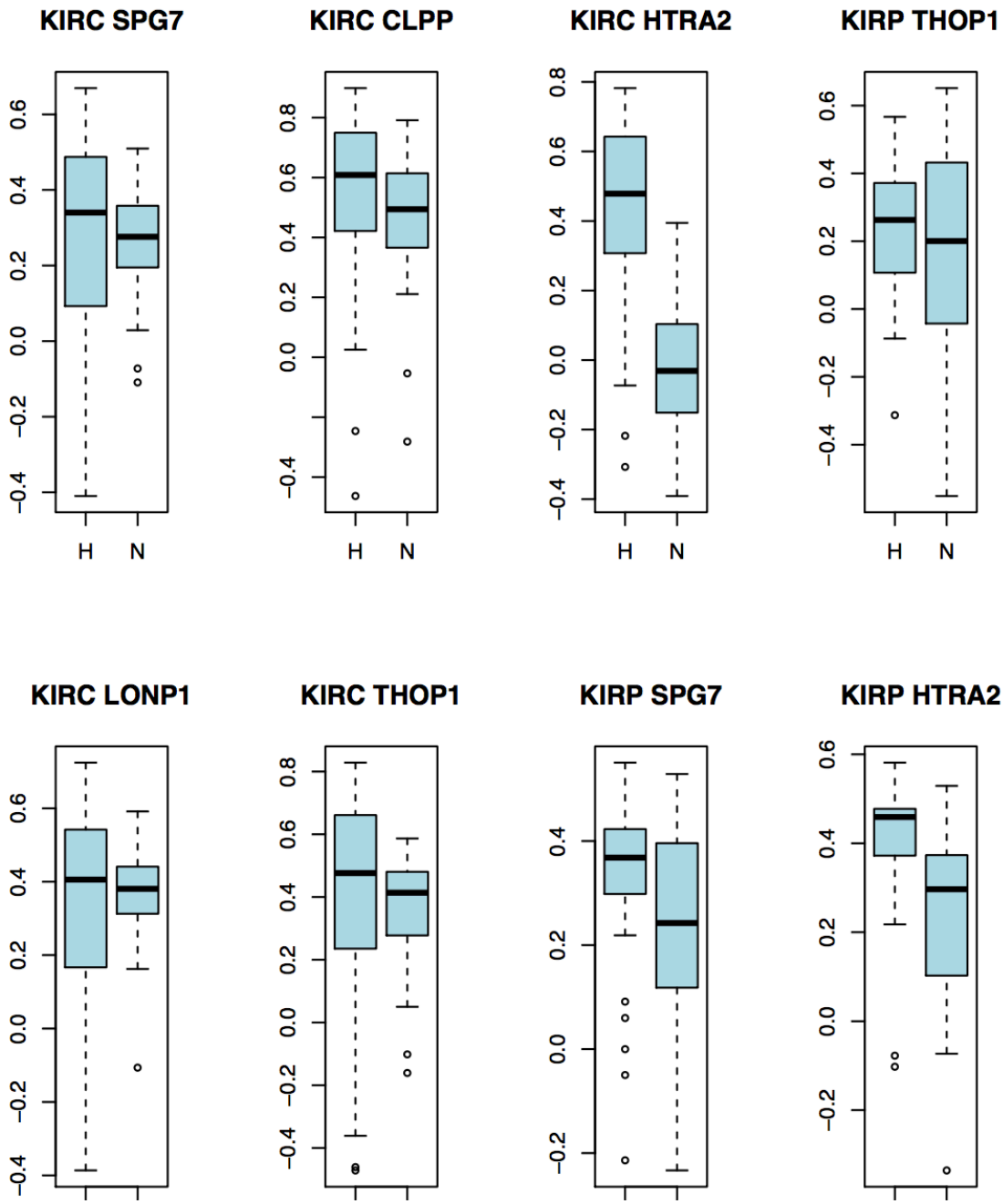
KIRC SPG7
KIRC CLPP
KIRC HTRA2
KIRP THOP1
KIRC LONP1
KIRC THOP1
KIRP SPG7
KIRP HTRA2
H
N

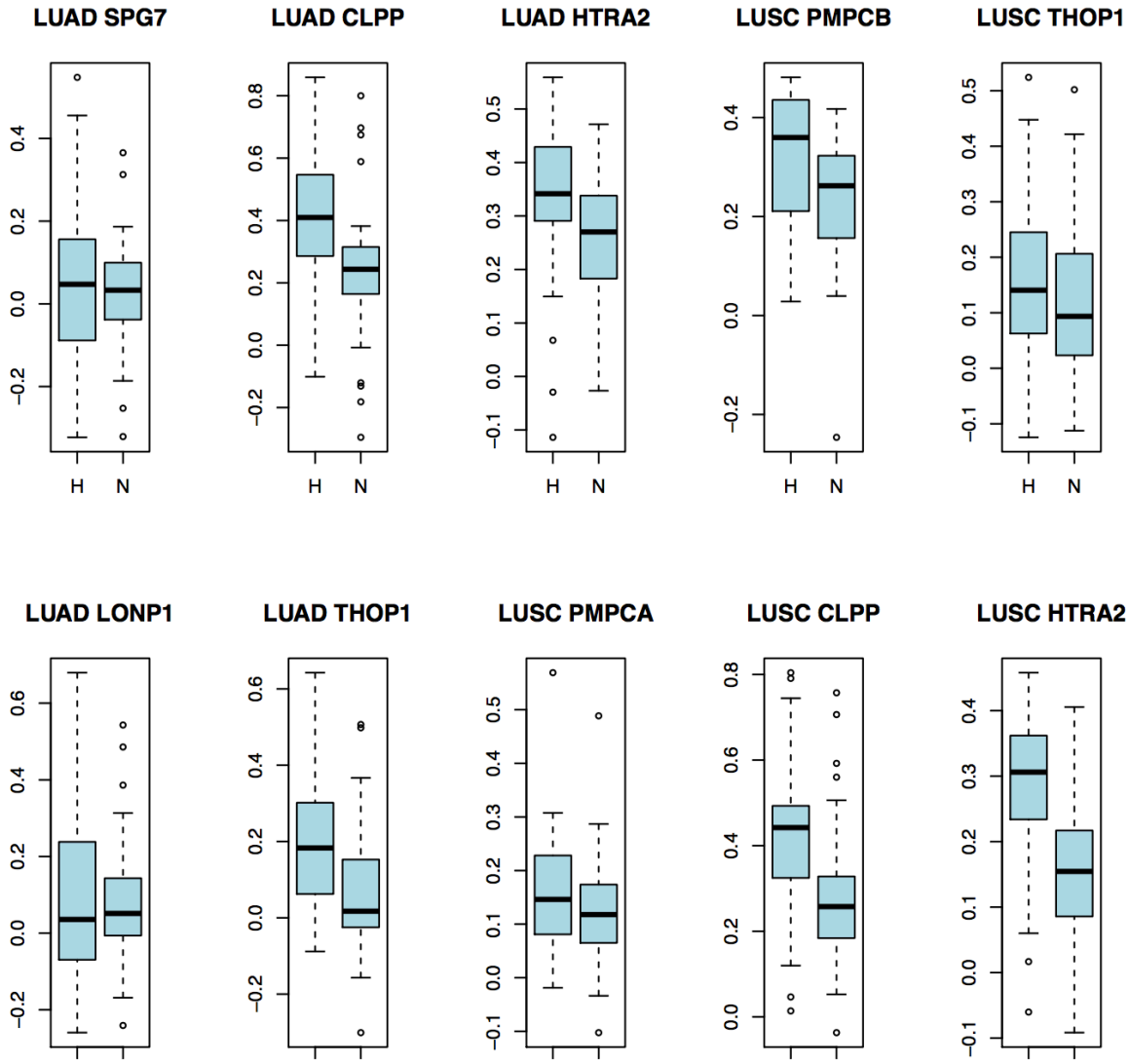
LUAD SPG7
LUAD CLPP
LUAD HTRA2
LUSC PMPCB
LUSC THOP1
LUAD LONP1
LUAD THOP1
LUSC PMPCA
LUSC CLPP
LUSC HTRA2
H
N

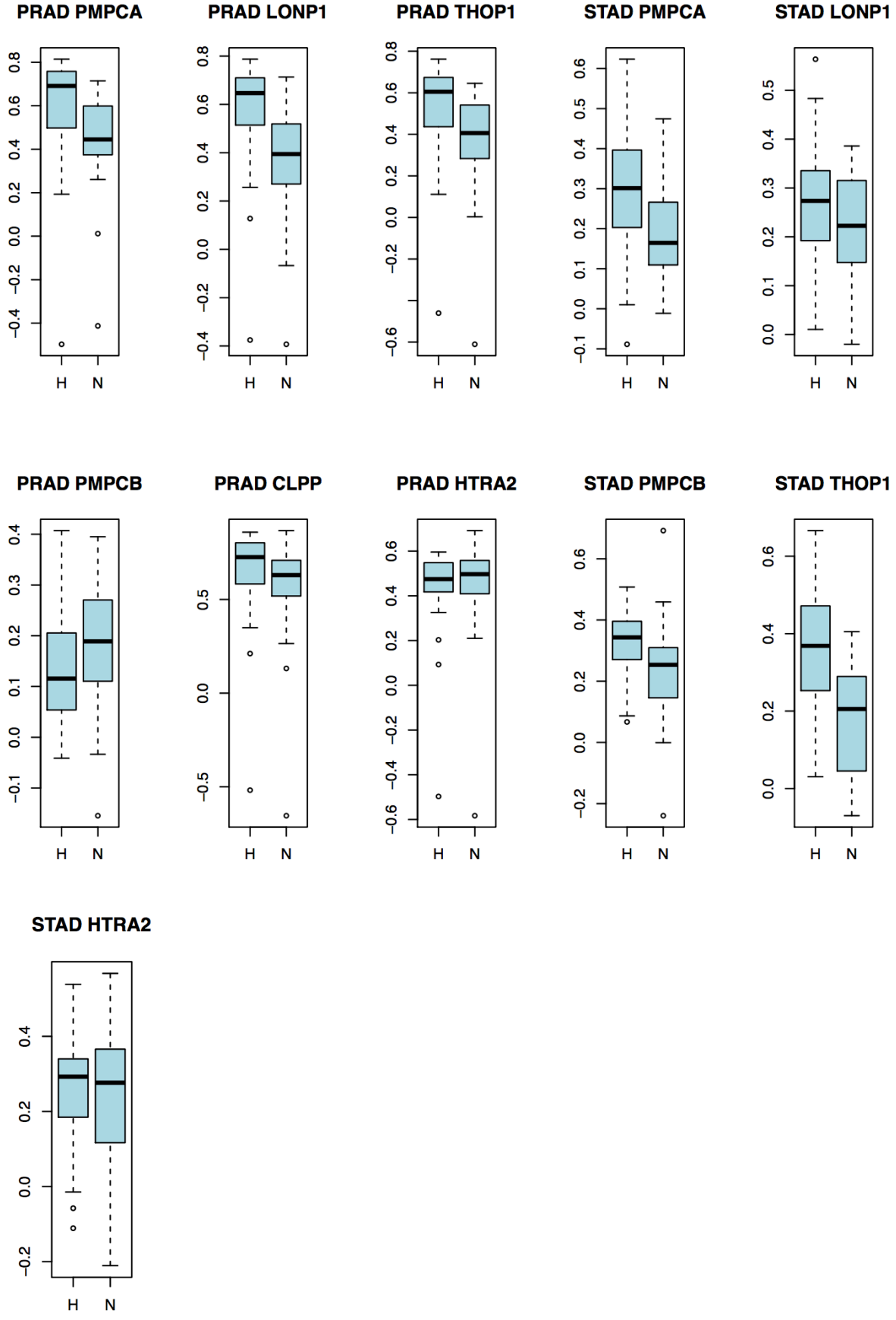
PRAD PMPCA
PRAD LONP1
PRAD THOP1
STAD PMPCA
STAD LONP1
PRAD PMPCB
PRAD CLPP
PRAD HTRA2
STAD PMPCB
STAD THOP1
STAD HTRA2
H
N

Figure S13: Correlation between predicted level of mitochondrial Fenton reactions (represented by CLPP) and Complex I (NDUF) and Complex III (COX) genes depends on the level of exogenous superoxide (reflected by NOX1 and NOX4) and the unreduced Fe^{3+} (reflected by FTL). CC represents the correlation coefficient between the expression of CLPP and that of each of the COX and NDUF genes, all averaged over samples of a specific stage.

BLCA	control	stage 1	stage 2	stage 3	stage 4	CC
CLPP	14.942916	16.31763	25.8732	24.590851	23.764957	
COX6B1	173.8874	208.49247	275.97722	248.13009	267.83816	0.9557774
COX7C	110.75447	109.77635	118.72459	112.04129	105.20528	0.3273254
COX8A	225.89148	249.96078	322.76147	307.90467	309.07451	0.9921989
NDUFA1	100.04768	153.72626	141.31709	122.73173	130.3538	0.3498118
NDUFB7	125.22632	136.0941	174.93108	159.86249	156.27573	0.9734474
NDUFS5	240.81127	255.01357	346.86923	358.2916	335.06819	0.9721345
FTL	2447.1578	2838.5314	3074.7082	3026.2596	2904.1788	
NOX1	0.7395838	0.741004	1.7670912	1.5617174	**1.1815257**	
NOX4	0.3232886	0.3747944	0.4094093	0.690071	**0.6400091**	
BRCA						
CLPP	11.300838	18.219754	19.751232	19.98095	22.350035	
COX6B1	109.47456	160.92965	176.56318	169.87742	163.40897	0.9107839
COX7C	80.447146	93.519207	93.648563	97.342277	101.98801	0.9846937
COX8A	127.21825	220.91167	223.69441	241.19895	296.70848	0.9764304
NDUFA1	76.40032	101.40438	107.13853	104.86038	126.96394	0.9868671
NDUFB7	82.083801	106.77511	115.00719	120.56463	125.12001	0.9606916
NDUFS5	169.11702	218.15271	235.44267	216.31295	262.13679	0.9543841
FTL	2596.0766	1924.0981	2058.4952	2269.1364	2360.5027	
NOX1	0.263673	0.4754631	0.5329026	0.5086471	**0.5390434**	
NOX4	1.4958499	1.7588185	1.7451599	1.9359141	**1.8859883**	
COAD						
CLPP	20.219546	34.655902	35.342646	32.097077	33.79039	
COX6B1	242.38998	218.78398	246.74345	235.0425	231.08975	-0.362562
COX7C	155.14427	117.19076	129.66093	116.67697	115.3078	-0.878049
COX8A	452.40651	331.4396	354.78707	341.90876	316.4015	-0.935792
NDUFA1	164.30971	128.76695	140.94566	128.76976	131.05189	0.9662224
NDUFB7	187.99042	177.88873	192.82755	183.92794	193.81644	0.0568345
NDUFS5	199.76779	271.96453	286.26394	272.3897	282.06823	-0.941514
FTL	2665.7728	1796.4598	2565.1898	3521.4798	3479.7353	
NOX1	42.048233	88.025222	80.0341	72.284962	**81.472576**	
NOX4	0.0465297	0.4358925	0.4432001	0.5552769	**0.4885946**	
ESCA						
CLPP	10.749054	14.95947	16.959927	14.730143		
COX6B1	96.652262	137.40348	164.00448	150.46055		0.9742682
COX7C	70.468228	63.829684	62.985889	67.883363		-0.896777
COX8A	206.96599	262.37959	271.43531	225.09811		0.8776362
NDUFA1	56.289762	77.324914	84.140788	85.79818		0.6369444
NDUFB7	78.384727	80.092402	92.765678	75.167262		0.7350623
NDUFS5	68.622909	167.14806	178.42633	211.97165		0.5323818
FTL	1388.9558	2060.9223	3503.2589	2432.1332		
NOX1	0.0929353	3.3608261	1.7409232	**1.5279468**		
NOX4	0.0490705	0.5457644	0.7843495	**0.9805316**		

HNSC	control	stage 1	stage 2	stage 3	stage 4	CC
CLPP	16.728095	17.547079	17.941146	19.473253	19.621051	
COX6B1	164.26882	127.89071	149.89768	157.78874	168.9238	0.359948
COX7C	97.17801	56.648854	62.934014	72.181185	71.968076	-0.31768
COX8A	303.59642	258.0913	273.74523	332.2769	285.11306	0.3606314
NDUFA1	96.09289	67.392808	81.548942	87.069034	89.562439	0.6750255
NDUFB7	132.0134	101.16562	112.94184	145.18818	131.04066	0.9446408
NDUFS5	203.04726	186.69417	216.98553	242.09681	236.65024	0.6596157
FTL	954.88756	1421.9542	1980.9933	2002.1379	2168.8056	
NOX1	0.3291178	0.2628965	0.3077033	0.338648	**0.3180447**	
NOX4	0.2138719	0.8222195	0.8254634	0.7709091	**1.0366844**	
KICH						
CLPP	23.094084	18.049127	22.35957	19.413519	22.125515	
COX6A1	118.83331	224.04609	250.35179	236.79496	239.18208	-0.40137
COX6B1	229.48637	299.47337	331.01968	299.97597	245.28932	-0.450635
COX7C	154.61233	244.49214	260.32717	303.39565	300.92998	-0.376147
COX8A	506.98596	713.28139	758.79267	772.49456	877.36875	-0.237341
NDUFA1	156.46223	206.46385	227.0973	214.10467	207.14728	0.8237396
NDUFB7	220.0634	256.47783	319.61096	299.66611	307.71678	0.8782659
NDUFS5	195.122	234.39082	220.88823	212.1389	239.49973	0.8120964
FTL	3170.5201	2258.7041	2177.8215	2967.037	3616.6752	
NOX1	0.2934175	0.2372122	0.2312495	0.193757	**0.2670463**	
NOX4	7.7396487	4.0461114	4.5428419	4.4293344	**2.925349**	
KIRC						
CLPP	16.119568	19.199038	19.144102	19.172136	20.082716	
COX6B1	163.47927	138.84356	168.00065	145.90994	158.06958	-0.326668
COX7C	142.2332	128.54127	148.99937	126.08533	134.67774	-0.355075
COX8A	323.26263	208.69418	261.28915	189.33482	211.36368	-0.863365
NDUFA1	138.64467	116.90029	131.64818	113.91322	128.88904	0.8854099
NDUFB7	127.57097	125.52971	176.65353	123.58479	131.63458	0.2581054
NDUFS5	164.29385	204.57414	211.29152	218.31011	237.01592	-0.829257
FTL	3333.1295	3423.5912	3487.659	3980.242	4033.1655	
NOX1	0.3094955	0.2772899	0.3340299	0.3175669	**0.3342995**	
NOX4	13.941776	5.8051246	6.236195	5.8114899	**5.7167528**	
KIRP						
CLPP	21.298224	21.157001	21.66218	22.448192	22.568847	
COX6B1	174.91654	216.27808	188.94627	265.42417	222.67956	0.6785387
COX7C	135.91757	166.26869	157.80994	171.34324	177.40753	0.6877712
COX8A	425.00097	308.82285	272.10266	316.11534	279.60296	-0.453856
NDUFA1	127.79709	172.74777	155.08733	159.88709	146.79827	-0.668857
NDUFB7	164.28448	199.89757	170.86011	196.28613	190.17657	-0.492599
NDUFS5	170.05818	306.62054	266.76627	283.93415	314.39824	-0.882579
FTL	4576.1657	5624.9518	8886.7296	6620.5624	5921.977	
NOX1	0.2860416	0.4471279	0.3677787	0.4146595	**0.4804371**	

LICH	control	stage 1	stage 2	stage 3	stage 4	CC
CLPP	15.785974	20.775879	21.49726	22.171337	20.972476	
COX6B1	113.75815	234.66793	298.96064	291.49905	283.30476	0.9712088
COX7C	77.725136	127.57968	143.85717	129.43429	135.65363	0.9504488
COX8A	155.32512	247.65985	290.44543	275.89145	329.60387	0.8688118
NDUFA1	72.086225	162.59506	195.5843	162.32373	166.54585	0.8786683
NDUFB7	110.05147	188.34542	274.85825	196.54115	249.39759	0.913661
NDUFS5	128.72519	188.85813	222.67755	220.81112	183.99404	0.751434
FTL	6020.6315	12355.5	14109.946	10092.137	19946.812	
NOX1	0.1464184	0.2971391	0.6240559	0.4458044	**0.3252532**	
NOX4	0.0216366	0.2286712	0.2574393	0.2428741	**0.1812129**	
LUAD						
CLPP	13.830214	16.539992	16.984501	17.772196	16.099594	
COX6B1	95.836583	164.35158	157.30743	176.08196	164.89465	0.938813
COX7C	78.343556	97.270026	98.94515	101.68028	96.380752	0.9776292
COX8A	175.71344	225.78288	233.81577	237.44653	257.68789	0.7725577
NDUFA1	70.24834	94.309942	96.992148	92.658242	93.045761	0.8850969
NDUFB7	90.753462	105.27662	110.26183	110.31709	95.304884	0.4701437
NDUFS5	132.71392	215.75023	211.06533	213.55178	210.76103	0.9055137
FTL	7583.1412	5413.5626	5232.9779	4742.052	4973.765	
NOX1	0.3020541	0.9717048	0.8373487	0.9302383	**0.6278999**	
NOX4	0.3441209	0.922339	0.945392	0.9061349	**0.7508919**	
LUSC						
CLPP	13.25864	19.615164	20.794974	21.116808	17.740273	
COX6B1	99.393286	201.84096	197.31599	229.96562	185.49643	0.9643161
COX7C	74.648809	72.684965	76.50704	79.540808	59.440724	0.2652234
COX8A	162.92172	278.51174	276.64462	297.33475	301.64496	0.8598766
NDUFA1	72.066995	104.37521	105.93633	107.08701	95.77976	0.902905
NDUFB7	88.437096	129.53708	122.22157	135.94888	122.07096	0.942391
NDUFS5	143.01194	235.76963	222.17286	219.09856	227.0046	0.9556697
FTL	7591.4645	5227.0022	4590.8801	5820.3704	5070.442	
NOX1	0.2579375	0.4688827	0.4983125	0.4103071	**0.2859415**	
NOX4	0.4036339	1.0801039	1.1297863	1.0422706	**1.6664054**	
PRAD						
CLPP	15.429243	20.974455	16.994207	15.5747	14.127958	
COX6B1	124.86412	157.53765	168.73114	169.8649	132.26267	0.4227885
COX7C	87.620662	113.07168	97.7802	88.853347	92.736534	0.9233218
COX8A	159.15822	252.57215	195.74153	181.56762	157.61574	0.9797246
NDUFA1	79.870496	113.09541	96.568984	107.01711	87.256747	0.8313084
NDUFB7	101.16446	150.85397	116.70147	115.22647	97.521285	0.9934154
NDUFS5	172.72853	198.74567	203.71578	226.3494	165.92802	0.432221
FTL	5152.8083	2538.1564	3301.7145	3518.6751	3951.5753	
NOX1	0.2698877	0.7805258	1.5415902	0.5523135	**0.2629**	

STAD	control	stage 1	stage 2	stage 3	stage 4	CC
CLPP	19.92029	19.488149	20.899901	19.011931	19.835184	
COX6A1	121.69359	108.15614	111.87911	103.13045	109.37649	0.4879864
COX6B1	256.37906	209.89114	217.94255	197.0001	192.46652	0.3286918
COX7C	119.28228	86.812276	93.447891	93.733101	94.062275	0.1243204
COX8A	410.5248	370.95758	345.36636	331.31943	358.28233	0.102055
NDUFA1	124.10362	101.81373	97.78112	92.93526	97.657691	0.9620645
NDUFB7	166.91373	111.0832	122.98352	112.55703	111.0423	0.8186908
NDUFS5	172.72853	198.74567	203.71578	226.3494	165.92802	-0.686792
FTL	2107.7856	2866.9728	3077.8187	3054.1219	2821.7903	
NOX1	0.1859404	3.3050159	4.2430486	6.1610974	**4.4023152**	
NOX4	0.1618863	0.4342618	0.679111	0.6228529	**0.6276138**	
THCA						
CLPP	15.475185	17.366509	18.393241	18.42894	17.54566	
COX6A1	66.723246	69.557413	85.906141	66.210645	62.205777	0.3859842
COX6B1	137.95149	150.06807	169.34652	156.89301	140.11371	0.7756814
COX7C	133.53948	132.30516	154.86275	137.07916	126.65022	0.4496665
COX8A	284.39276	253.88411	336.02714	241.12013	214.91843	0.0067403
NDUFA1	115.7663	93.369823	112.82326	90.849493	78.540813	0.8893692
NDUFB7	157.59081	148.06797	179.02764	154.39006	130.71742	0.9481718
NDUFS5	203.77134	283.20913	296.51791	291.25277	275.14498	-0.044464
FTL	1971.5174	1915.9494	1755.7707	2049.3661	1824.3684	
NOX1	0.2605549	0.478036	0.4179708	0.4589784	**0.485354**	
NOX4	0.2165369	1.1020347	0.9307647	1.3923064	**1.3247737**	

Figure S14: Unreduced Fe^{3+} in mitochondria as reflected by the HSCB and the ABCB6 genes across 14 cancer types. The ones highlighted in red represent those not up-regulated in cancer compared to the controls.

Cancer type	Gene	Control	Stage 1	Stage 2	Stage 3	Stage 4
BLCA	HSCB	6.88151922	7.310628495	8.993340048	8.481314482	7.548306992
	ABCB6	1.59990777	1.233107232	1.417232986	1.4569098	1.332567181
BRCA	HSCB	7.390967902	7.441224387	7.537135362	7.552662764	7.780806437
	ABCB6	1.039059748	1.100508881	1.191606265	1.250196908	1.52382711
COAD	HSCB	5.980135117	6.393129161	6.518328854	5.996200995	5.51669913
	ABCB6	0.443637709	1.004842716	1.039029129	1.076627101	1.071552624
ESCA	HSCB	3.390608364	4.404148628	4.939685898	4.688559931	
	ABCB6	0.225776623	1.511963068	2.547655094	1.46365758	
HNSC	HSCB	5.573766519	5.700525211	5.699113601	7.152921464	6.671429631
	ABCB6	1.076750721	1.530173529	1.667070613	1.728425996	1.825877634
KICH	HSCB	7.771310094	5.859905424	6.372265277	6.09203463	8.740121458
	ABCB6	0.586380364	0.206931162	0.191544164	0.149209045	0.456614249
KIRC	HSCB	6.038629697	8.267559324	8.440878453	8.239120885	9.067288653
	ABCB6	0.641922862	2.162305238	2.064931643	2.26210016	2.493865033
KIRP	HSCB	6.684949025	7.51316929	7.534889408	6.552381118	8.555873934
	ABCB6	0.809280397	1.441540516	1.754945461	2.192579424	2.938284679
LICH	HSCB	7.367050184	10.19233653	9.187640167	10.38056538	11.24318158
	ABCB6	1.151797331	2.120299986	2.410861794	2.700993509	3.67082284
LUAD	HSCB	5.556556233	8.365701812	8.490273927	8.459511829	7.424806429
	ABCB6	0.458242475	2.025467779	2.018634183	1.882411236	2.807316677
LUSC	HSCB	5.3864707	9.580620274	9.372425413	9.567280994	8.150435159
	ABCB6	0.480757783	3.240348245	2.763514941	3.285640255	2.227407803
PRAD	HSCB	6.012267639	6.593592328	6.115267576	6.19098412	6.13873376
	ABCB6	0.672609053	1.051751337	0.94135658	0.803105134	0.71489075
STAD	HSCB	5.12460935	5.534552887	5.269292256	4.998124005	4.651254497
	ABCB6	0.564738332	1.017207449	0.970908023	0.949561899	0.934737417
THCA	HSCB	8.252546862	8.717546762	8.542094272	8.772438043	7.941691876
	ABCB6	1.406559737	1.0529645	1.094546024	0.940086591	0.862476859

Figure S15: mitochondrial Fenton reactions contribute to ATP syntheses. We have used CLPP and CLPX reflect the level of mitochondrial Fenton reactions, and ATB5B for ATP synthase, plus UCP5 (SLC25A14) and UCP2 genes. The coloring scheme is the same as in earlier figures, e.g., Figure S10.

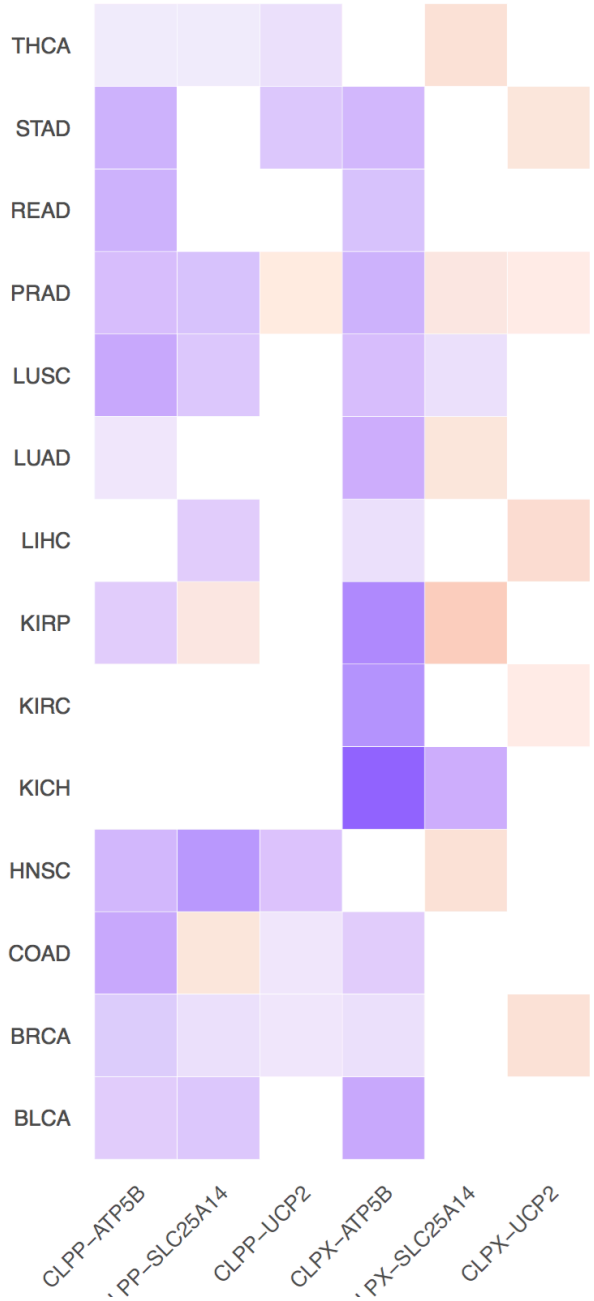

Figure S16: Gene-expression levels of SOD3, and extracellular hydrogen peroxide and superoxide producing genes in 16 inflammatory diseases and 14 cancer types. The coloring scheme is the same as in earlier figures, e.g., Figure S10.

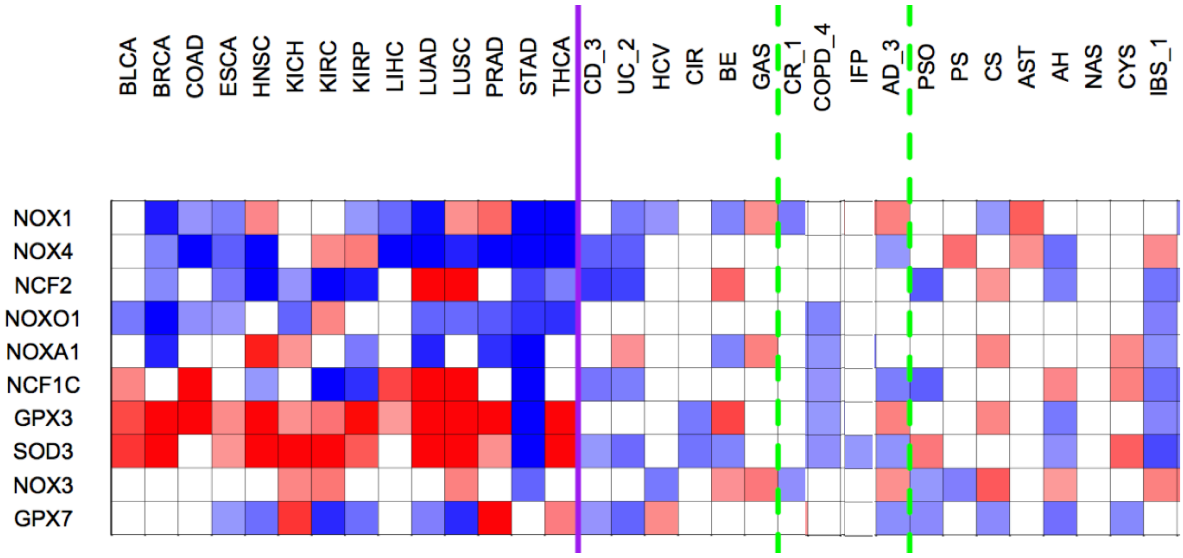

Figure S17: Staining score comparison between up-regulated genes and the background genes in eight cancer types. Bar on the left (B_G) is the staining score for background genes and bar on the right (M_G) is the score for the up-regulated model genes.

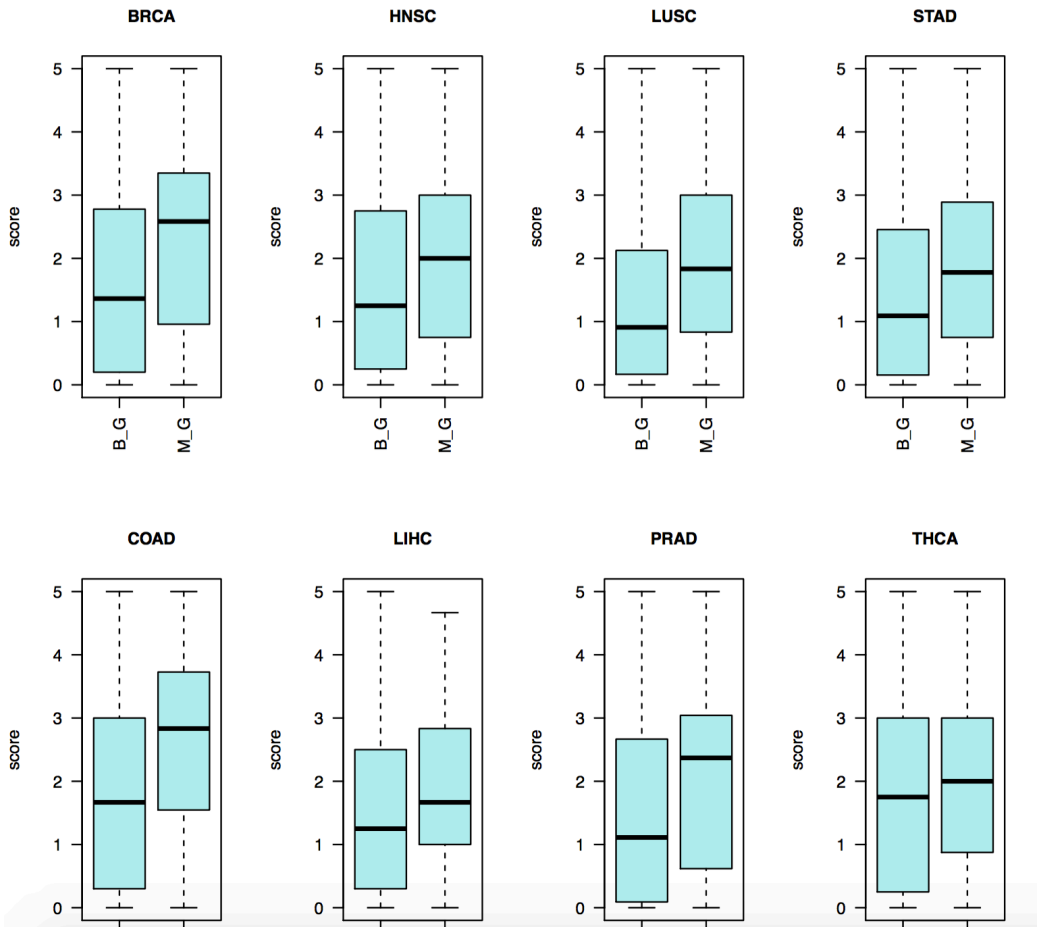

D. SUPPLEMENTARY TABLES AND CAPTIONS

TABLE S1: All genes used to demonstrate the occurrence of Fenton reactions in cytosol and mitochondria along with the related analysis results. CY model genes: genes initially used to establish Fenton reactions in cytosol. CY selected genes: genes selected from the model genes that give the optimal R^2 values. CY permutation 1 and 2 are the statistical significance of the derived R^2 values against sets of genes with comparable expression profiles with those in CY selected genes. Similarly defined are for the mitochondrial genes. ECM MMPs, component and glycosaminoglycan are the MMP, glycosaminoglycan and collagen genes used to establish Fenton reactions in extracellular matrix. ECM correlation: correlation between MMP and ECM copper containing genes.

[Table S1 should be here.]

TABLE S2: The first column is cancer type and the second column is the statistical significance of the contribution by glycolytic pyruvate towards non-lactate production in Figure S7.

Cancer type	p-value
BLCA	6.54E-02
BRCA	6.33E-02
COAD	1.13E-09
ESCA	4.33E-01
HNSC	1.30E-03
KICH	6.55E-02
KIRC	5.40E-85
KIRP	5.49E-52
LIHC	2.59E-07
LUAD	5.93E-01
LUSC	1.12E-02
PRAD	7.07E-01
STAD	3.08E-02
THCA	1.60E-01

TABLE S3: Gene-expression analysis data in support of Fenton reaction reactions in cytosol, mitochondria and ECM.

[Table S3 should be here.]

TABLE S4: Differential expression analyses of Fenton reaction-related genes, where a differentially expressed gene is determined by Mann-Whitney Test with FDR < 0.05. In the table, duplicated genes in microarray data refer to different probes of the same gene.

[Table S4 should be here]

REFERENCES

Adam, F.I., Bounds, P.L., Kissner, R., et al. (2015). Redox Properties and Activity of Iron–Citrate Complexes: Evidence for Redox Cycling. Chemical research in toxicology *28*, 604-614.

Aran, D., Sirota, M., and Butte, A.J. (2015). Systematic pan-cancer analysis of tumour purity. Nature communications *6*.

Brown Jr, R.H. (1997). Superoxide dismutase and oxidative stress in amyotrophic lateral sclerosis. Cold Spring Harbor Monograph Archive *34*, 569-586.

Cao, S., Zhang, C., and Xu, Y. (2015). Somatic mutations may not be the primary drivers of cancer formation. International journal of cancer *137*, 2762-2765.

Chen, C., and Paw, B.H. (2012). Cellular and mitochondrial iron homeostasis in vertebrates. Biochimica et Biophysica Acta (BBA)-Molecular Cell Research *1823*, 1459-1467.

Flamholz, A., Phillips, R., and Milo, R. (2014). The quantified cell. Mol Biol Cell *25*, 3497-3500.

Friedman, J., Hastie, T., and Tibshirani, R. (2010). Regularization paths for generalized linear models via coordinate descent. Journal of statistical software *33*, 1.

Hamada, Y.Z., Carlson, B., and Dangberg, J. (2005). Interaction of malate and lactate with chromium (III) and iron (III) in aqueous solutions. Synthesis and Reactivity in Inorganic and Metal-Organic Chemistry *35*, 515-522.

Hirayama, A., Kami, K., Sugimoto, M., et al. (2009). Quantitative metabolome profiling of colon and stomach cancer microenvironment by capillary electrophoresis time-of-flight mass spectrometry. Cancer Res *69*, 4918-4925.

Kami, K., Fujimori, T., Sato, H., et al. (2013). Metabolomic profiling of lung and prostate tumor tissues by capillary electrophoresis time-of-flight mass spectrometry. Metabolomics *9*, 444-453.

Lu, M., Zhou, L., Stanley, W.C., et al. (2008). Role of the malate–aspartate shuttle on the metabolic response to myocardial ischemia. Journal of theoretical biology *254*, 466-475.

Park, M.Y., and Hastie, T. (2007). L1 ‐ regularization path algorithm for generalized linear models. Journal of the Royal Statistical Society: Series B (Statistical Methodology) *69*, 659-677.

Richardson, D.R., Lane, D.J., Becker, E.M., et al. (2010). Mitochondrial iron trafficking and the integration of iron metabolism between the mitochondrion and cytosol. Proc Natl Acad Sci U S A *107*, 10775-10782.

Safran, M., Dalah, I., Alexander, J., et al. (2010). GeneCards Version 3: the human gene integrator. Database *2010*, baq020.

Saleh, A.M., Rombola, G., and Batlle, D.C. (1991). Intracellular H+ buffering power and its dependency on intracellular pH. Kidney Int *39*, 282-288.

Subramanian, A., Tamayo, P., Mootha, V.K., et al. (2005). Gene set enrichment analysis: a knowledge-based approach for interpreting genome-wide expression profiles. Proceedings of the National Academy of Sciences *102*, 15545-15550.

Wang, J.D., and Levin, P.A. (2009). Metabolism, cell growth and the bacterial cell cycle. Nature reviews. Microbiology *7*, 822-827.

Wingender, E., Dietze, P., Karas, H., et al. (1996). TRANSFAC: a database on transcription factors and their DNA binding sites. Nucleic acids research *24*, 238-241.